MUD-FILTRATE INVASION MODELING TO QUANTIFY STATIC AND DYNAMIC PETROPHYSICAL PROPERTIES OF FRACTURED AND VUGGY CARBONATE FORMATIONS

by

Luis Javier Miranda, B.S.

Thesis

Presented to the Faculty of the Graduate School of
The University of Texas at Austin
in Partial Fulfillment
of the Requirements
for the Degree of

Master of Science in Engineering

The University of Texas at Austin
August 2008

MUD-FILTRATE INVASION MODELING TO QUANTIFY STATIC AND DYNAMIC PETROPHYSICAL PROPERTIES OF FRACTURED AND VUGGY CARBONATE FORMATIONS

Approved by
Supervising Committee:

Supervisor: Carlos Torres-Verdín

Jerry Lucia

Dedication

I dedicate this thesis to our God Almighty, who has continuously guided me in all my endeavors.

I dedicate this thesis to my parents Luis and Graciela, who have offered me unconditional love and support throughout my life.

I dedicate this thesis to my wife Libsen for her love, support, your laughter, and everything else we share together each day.

I dedicate this thesis to my son Elliott and my daughter Antonella; you both are the inspiration in everything I do.

Thanks to you all for being so patient and supporting to me while I have spent untold periods of time away from you working on this research.

Acknowledgements

From the formative stages of this thesis, to the final draft, I owe an immense debt of gratitude to my supervisor Dr. Carlos Torres-Verdín. He provided a worthy support and encouragement during the research and writing of this thesis. His sound advice and careful guidance were invaluable.

I am thankful to PDVSA (Petróleos de Venezuela, S.A.) for providing the data used in the case studies and for the support and permission to publish our results. I thank also PDVSA for bestowing upon the author a scholarship in 2006 to pursue a Master of Science in Engineering.

The work reported in this thesis was partially funded by The University of Texas at Austin's Research Consortium on Formation Evaluation, jointly sponsored by Anadarko, Aramco, Baker Atlas, BHP Billiton, BP, British Gas, Chevron, ConocoPhillips, ENI E&P, ExxonMobil, Halliburton, Hydro, Marathon, Mexican Institute for Petroleum, Occidental Petroleum, Petrobras, Schlumberger, Shell International E&P, Statoil, TOTAL and Weatherford.

I thank Prof. Jerry Lucia not only for being the second reader of this thesis, but also for the valuable comments and discussions sustained during this research.

Special acknowledgment is extended to the reservoir studies group of Barinas District of PDVSA South Division for all the help in collecting the data needed throughout this research.

And lastly, but certainly not least, I thank Jesus Salazar for his useful technical comments and support during this research, Hee Jae Lee for his help with the UTFET simulator and technical advice at any time, and Renzo Angeles for his support and help during my time at The University of Texas at Austin. I also express my gratitude to the faculty and staff of the Department of Petroleum and Geosystems Engineering for their guidance during my two years as an MS student. All my family and friends in Venezuela and my new friends here in Austin also deserve to be acknowledged for their support, understanding and encouragement during the development of my studies and this research.

August 2008

Abstract

MUD-FILTRATE INVASION MODELING TO QUANTIFY STATIC AND DYNAMIC PETROPHYSICAL PROPERTIES OF FRACTURED AND VUGGY CARBONATE FORMATIONS

Luis Javier Miranda, M.S.
The University of Texas at Austin, 2008

Supervisor: Carlos Torres-Verdin

We develop and validate a new method to estimate secondary porosity and effective permeability of fractured and vuggy carbonate formations based on the numerical simulation of the process of mud-filtrate invasion. The method includes the geological characterization of core measurements and their integration with well logs and fluid production measurements. Applications of the new method are focused to the interpretation of data acquired in a carbonate reservoir in the Barinas-Apure Basin in southwest Venezuela, which is a triple-porosity system exhibiting inter-crystalline, intra-crystalline, moldic, vuggy (connected and non-connected) and fractured porosity, all embedded in a tight matrix. Rock-core data and image logs indicate that vugs are the mayor component of secondary porosity whereas fractures and interconnected vugs account for most of the permeability.

The initial phase of our method consists of integrating core measurements with conventional and non-conventional well logs to calculate static and dynamic petrophysical properties via formation evaluation methods typically used to assess carbonate formations. Starting with the petrophysical variables calculated from standard formation-evaluation procedures, we simulate the process of invasion with both water- and oil-base muds. Resulting spatial distributions of water saturation and salt concentration give rise to spatial distributions of electrical resistivity which are used to calculate laterolog and induction logs. Comparison of simulated logs and measurements provides an effective means to assess whether the petrophysical properties calculated with standard interpretation methods are reliable. Specifically, if the calculated values of porosity and permeability are not correct the simulation of mud-filtrate invasion and resistivity logs will yield a poor match with measurements. In such cases, we update both variables until securing a good match between measurements and simulations. We find that permeability and porosity values estimated with our method reproduce values observed for the entire fluid-flow network system (well test data and core observations).

Differences between simulations are measurements are diagnostic of presence of vugs and/or fractures. This procedure was tested on several key wells with and without core measurements, borehole images, and well-testing measurements. We conclusively find that our updated values of porosity and permeability are in very good agreement with the properties of the global petrophysical system. Differences between porosity and permeability values before and after simulation of the process of invasion are reliable indicators of presence and influence of vugs and/or fractures in the displacement of hydrocarbons by mud filtrate.

Table of Contents

List of Tables

List of Figures

CHAPTER 1

Introduction

Permeability estimation is one of the most important steps of reservoir characterization. Even though there are reliable methods to estimate rock properties such as porosity and fluid saturation, permeability, a tensorial property, remains the most difficult to estimate, especially in carbonate reservoirs.

In heterogeneous reservoirs with variable rock composition and petrophysical properties, integration of core and log information is needed to predict properties in zones with no or scarce petrophysical information. Core measurements and well logs are useful in reservoir characterization if they are tied to geological models.

In this thesis, estimation of permeability is performed via numerical simulation of the process of mud-filtrate invasion that takes place in complex reservoirs with a triple-porosity system (Figure 1.1) by considering the simulation of dual-laterolog and array-induction resistivity logs to validate the estimation of reservoir properties.

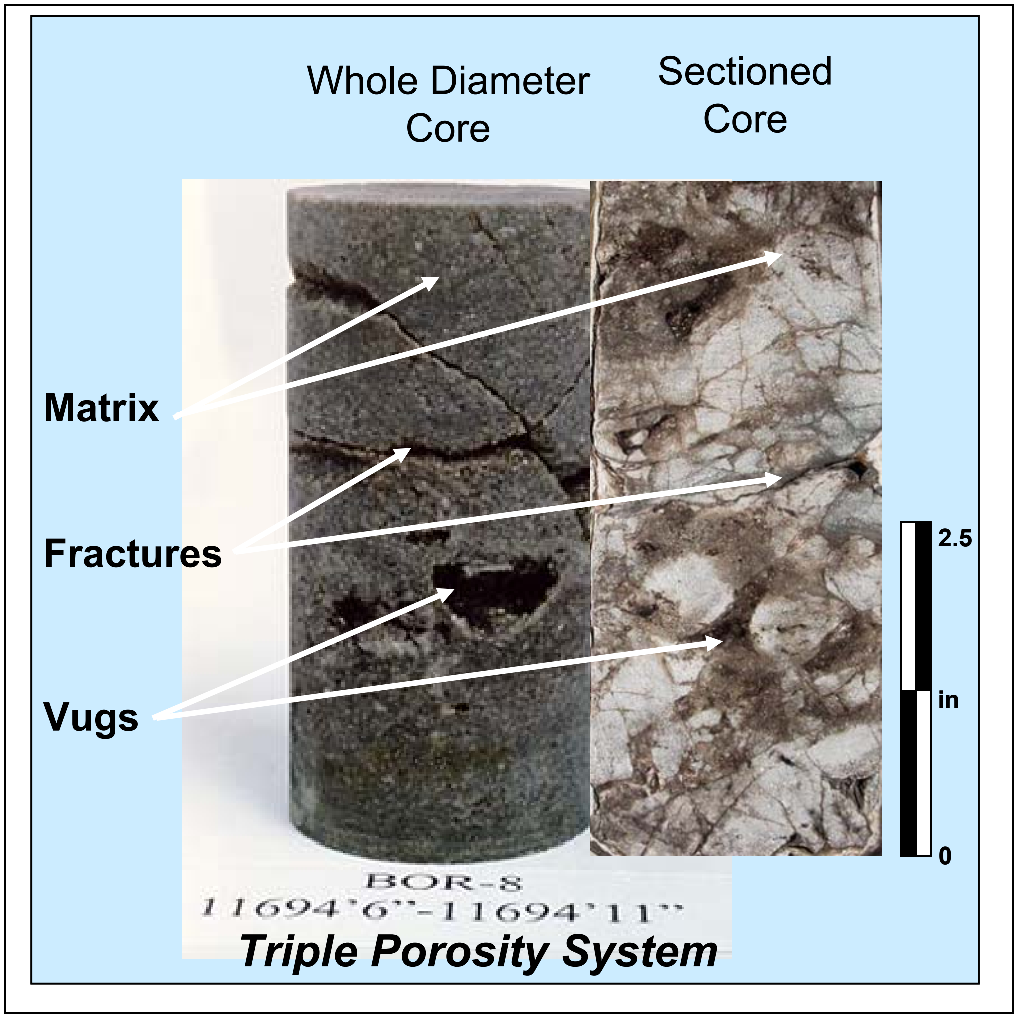

Figure 1.1. Typical distribution of porosity in the "O BOR-2E" reservoir. The rock matrix is very tight, exhibiting porosities from 2 to 14% in this case, whereas matrix permeability varies between 0.01 mD and 18 mD.

Our method includes the geological characterization of core measurements and its integration with well logs and production data. We consider field data acquired in a reservoir located in the Barinas-Apure petroleum basin of Southwest Venezuela, which is a significant hydrocarbon producer in the Borburata Field. Facies in this reservoir consist of sandstone, mixed sandstone-dolostone, dolostone, pelecypod limestone, foraminiferal limestone-siltstone, and shale. Sedimentological studies describe these facies to represent deposition in a shallow-marine carbonate platform environment (Kupecz et al, 2000; Mendez, 2002). The amount of each facies varies depending on the zone across the field. One of the most important observations is that the best oil-producing wells are located in zones with large amounts of dolomite which display an increase in secondary porosity (interconnected vugs and fractures). Compared to previous characterizations of the same reservoir (Kupecz et al, 2000), our preliminary results show that the new method to estimate permeability is reliable in reservoirs with secondary porosity (vugs and fractures). Furthermore, the estimated permeability agrees better with the one obtained from pressure transient tests (which is believed to be a good representation of the triple-porosity system). We performed the above estimation with the integration of all available information, thereby reducing uncertainty associated with other interpretation methods.

1.1 OBJECTIVE

The main purpose of this study is to diagnose and estimate secondary porosity and permeability in fractured and vuggy carbonate formations based on the numerical simulation of the physics of mud-filtrate invasion, and corresponding effect on resistivity logs.

1.2 PREVIOUS WORK

A wide variety of methods to estimate permeability have been described in the literature. These methods are based on correlations between permeability, porosity, irreducible water saturation, pore throat, etc. Kozeny (Tiab and Donaldson, 2004) developed the first correlation between permeability and porosity and grain surface area. Reliable results of permeability estimation can be obtained in reservoirs with uniform grain packing, which are uncommon. Kozeny's relationship can be applied only in cases where special core analysis is available.

Tixier (1949) introduced a method to estimate permeability from resistivity gradients. He used empirical relationships between resistivity and water saturation, water saturation and capillary pressure, and capillary pressure and permeability. Because this method estimates permeability from resistivity gradients, it has important limitations. For example, the predicted permeability is obtained as an average for zones with the same resistivity gradient. In addition, reliable estimation of oil-water contacts has to be performed from logs together with a prediction of hydrocarbon density at reservoir conditions.

Using the Tixier relationship, Wyllie and Rose (1950) proposed an expanded empirical equation that relates permeability with capillary pressure, water saturation, cementation exponent and formation factor. This method can be applied only when meeting some restricting assumptions: (a) the minimum water saturation calculated in a reservoir is the same as irreducible water saturation; (b) irreducible water saturation is a function of grain surface area. Moreover, Willie and Rose indicated that permeability values obtained through their correlation “cannot, however, be expected to have more than an order of magnitude significance”.

Timur (1968), based on previous work of Kozeny and Willie and Rose, proposed an equation based on the relation between permeability, porosity, irreducible water saturation, and three statistically determined parameters. This empirical relationship was developed using information from reservoirs in North America. It assumes that the cementation factor is 1.5 for all cases, which is not true for many reservoirs around the world. In addition, this equation can only be used with measurements of residual water saturation.

Coates and Dumanoir (1974) proposed an empirical method to improve the estimation of permeability. This method is based on the relation between permeability, porosity, water saturation, formation resistivity at irreducible water saturation. It also includes an exponent that is derived from cementation and saturation exponents based on core and log analysis. Despite the fact that this method offers better estimates of permeability, it has some limitations. For instance, Coates and Dumanoir’s equation is applicable to clean formations with API (America Petroleum Institute) oil gravity of 45 (light oil). In cases where API oil gravity is not 45, it can be adjusted with a correction factor introduced by Coates and Dumanoir. This method can be used if the reservoir is at irreducible water saturation. To overcome the latter, they introduced a correction factor. The importance of the approach is that it is the first method that meets the condition of zero permeability at zero porosity, when irreducible water saturation is 100%. Furthermore, this methodology can be used in shaly formations and those that are not at irreducible water saturation if the given corrections are considered.

Coates and Denoo (Babadagli et al., 2004) proposed a relationship between permeability, porosity, and irreducible water saturation. This equation satisfies the condition of zero permeability at zero porosity but can only be applied to formations that are at irreducible water saturation.

Windland model (Pittman, 1992) is considered a reliable way to predict reservoir performance. It relates permeability with pore throat radius obtained from capillary pressure curves. Pore throat radius is an important parameter estimating permeability. However, it is not the only one. This consideration could yield different permeability values. The Windland relation also assumes theoretical tubes/pore throats that do not exist in the reservoirs. The model is considered very popular in the oil industry despite its limitations.

Lucia (1999) introduced a relationship to predict permeability designed for carbonates and based on relations between permeability, porosity, particle size/rock fabric, rock type, etc. Even though this model can be used for the estimation of matrix permeability, it is not suitable for the case of touching-vug pore systems in carbonate.

Salazar et al. (2006) assessed permeability from well logs based on core calibration and simulation of mud-filtrate invasion. Good results were obtained for the case of clastic reservoirs.

Since the late 1990s, additional methods have been used such as application of artificial neural networks, fuzzy logic, multiple variable regression, and other algorithms to relate known properties of the reservoir and to estimate permeability.

1.3 METHOD OF CORE-LOG INTEGRATION

Many empirical methods to estimate permeability are available today. These methods are based on the correlation between permeability, porosity, irreducible water saturation, pore throat radius, etc. According to Babadagli and Al-Salmi (2004) these methods can be grouped into two categories: Pore-scale models and field-scale models. Most of the studies at the pore-level were performed on clastic rocks where the grain and pore properties could be modeled quantitatively. The application of these pore-scale models in carbonate rocks is debatable because of their dependence on pore and grain properties. Thus, in general it is difficult to perform an accurate characterization in complex carbonate reservoirs through grain and pore characteristics (Babadagli and Al-Salmi, 2004). Implementation of improved techniques and integration of core and log data is necessary to obtain reliable estimates of permeability from well-log information. In our case, the application and analysis of core data is required to improve the estimations.

Some of the methods discussed in the literature (Jennings and Lucia, 2003; Salazar et al, 2006; Babadagli and Al-Salmi, 2004; Hurley, 1998; and Gomaa et al, 2006) are studied to determine their applicability to this study of carbonate reservoirs. We need a new approach because there is a large variability of rock composition and petrophysical properties. We also need to consider the heterogeneity present in the lithology of this reservoir.

In this thesis, we first considered and implemented a definition of rock types and established a relationship with the geological model (structural and stratigraphic), facies, and distribution of petrophysical properties. Second, we quantified the influence of mud-filtrate invasion on the spatial distribution of fluids in permeable rocks around the wellbore using the properties obtained from well logs and core-log integration. The analysis performed on key wells was reliable because of the abundance of information in these wells, such as core measurements, special logs and pressure transient measurements. They enabled the comparison of results against data acquired at different scales.

Third, the results obtained in the first approach were adjusted considering reservoir properties of the complete system (matrix + vugs + fractures) observed in rock-core measurements and in non-conventional well logs. This provided the estimation of secondary porosity (vugs and fractures), and an accurate estimation of permeability in the carbonate reservoir. Our method includes a step-by-step procedure. We propose a method at in-situ that considers a bigger piece of the rock; therefore, it accounts the presence of vugs, fractures and matrix.

We find that permeability and porosity values estimated with our method reproduce values observed for the entire fluid-flow network system (well test data and core observations). Differences between simulations and measurements are diagnostic of presence of vugs and/or fractures. This procedure was tested on several key wells with and without core measurements, borehole images, and well-testing measurements. We conclusively find that our updated values of porosity and permeability are in very good agreement with the properties of the global petrophysical system. Differences between porosity and permeability values before and after simulation of the process of invasion are reliable indicators of presence and influence of vugs and/or fractures in the displacement of hydrocarbons by mud filtrate.

CHAPTER 2

Review of Field Data and Information Available

We present a general description of the Borburata Field and “O BOR 2E” reservoir in this chapter. This part of the report also describes all the data available for the study including the geological background of the reservoir under consideration.

2.1. GENERAL DESCRIPTION OF THE HYDROCARBON FIELD

Figure 2.1 shows the reservoir “O BOR 2E” of Borburata Field, located in the Barinas-Apure petroleum basin of Southwest Venezuela. The field, with a total area of 14 Km^2 (3459 Acres), is formed by a group of smaller zones delimited by faults. There are two other reservoirs in Borburata Field, “Gobernador” and Escandalosa “P.” However, the carbonate reservoir produces most of the hydrocarbon of the Borburata Field. This field was discovered in 1994 when the well BOR-2E was completed in “O BOR 2E” reservoir. It has a large variability of rock composition and petrophysical properties, with a high grade of heterogeneity present in the lithology of the reservoir.

This carbonate reservoir is formed of a triple-porosity system (Matrix + Vugs + Fractures), according to observations and analysis of rock-core measurements and non-conventional well logs data. There are other fields that have produced from “O BOR 2E” reservoir. However, Borburata field has the highest cumulative and current production. Furthermore, the amount of secondary porosity existing in the field has not been observed in any other field in Barinas basin making it the most prospective one in the entire area.

Figure 2.1 shows the grade of quality prospects for each field that is presented in the scale of colors from high to low quality prospects.

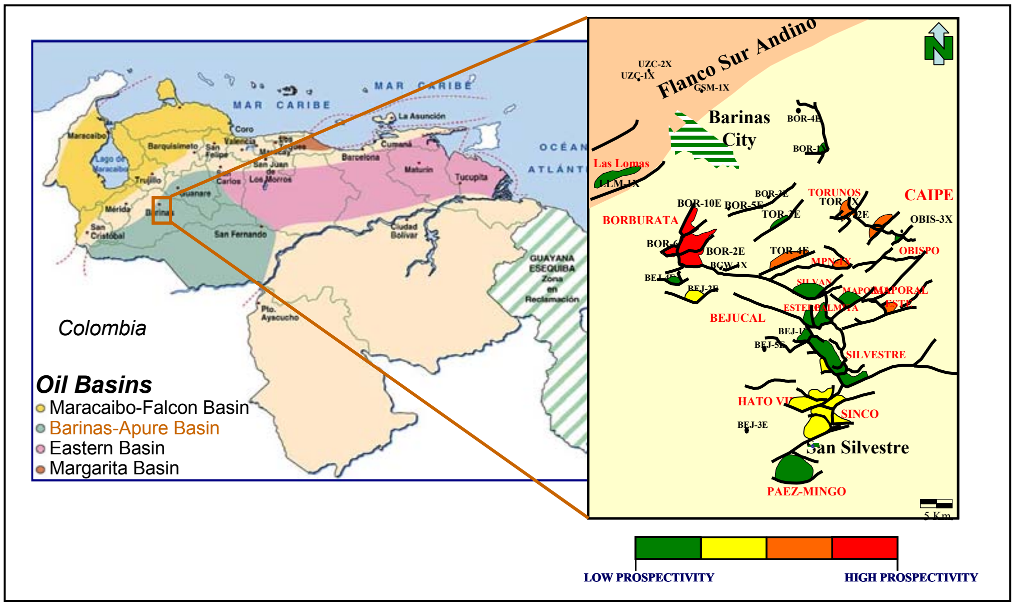

Figure 2.1. Map showing the field location in the Barinas-Apure petroleum basin of Southwest Venezuela. Colors indicate the high and low quality prospects in Barinas area. The Borburata field is showed in red.

2.2 WELL-LOG INFORMATION

During the production of Borburata field, a considerable amount of well logs has been acquired including conventional and advanced well logs (Image, full wave sonic, nuclear magnetic resonance, dipmeter, formation tester and sampling, VSP, check shots). Appendix A contains a detailed inventory of well logs available for this reservoir. Figure 2.2 shows the characteristic response for the most important well logs. Resistivity logs have been acquired with water-based mud (WBM) and oil-based mud (OBM). Dual

Laterolog Tool (WBM), High-Resolution Laterolog Array Tool (WBM), Dual Induction (OBM) and Array Induction Log (OBM) are some of the resistivity logs available.

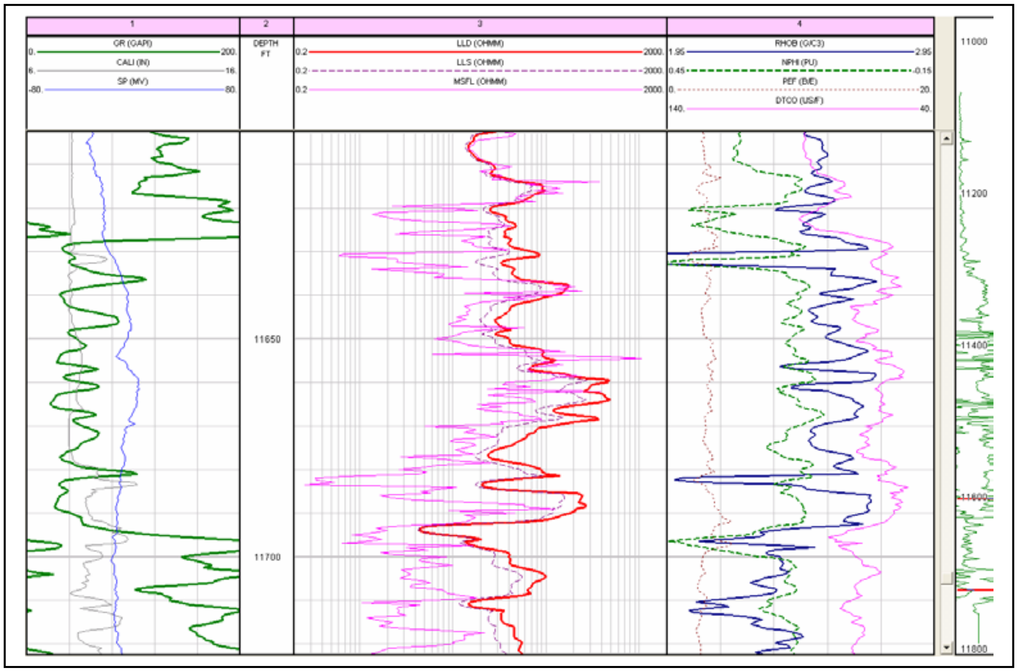

Figure 2.2. Typical set of well logs acquired in the "O BOR-2E" reservoir. Track 1: Lithology logs and borehole quality control. Track 2: Dual Laterolog resistivity logs and Micro Spherical Focus Log. Track 3: Porosity logs including Neutron, Formation Density, and Sonic. Track 4: Gamma ray log acquired in all the intervals of interest.

2.3 ROCK-CORE MEASUREMENTS

Four cores were acquired in this reservoir: BOR-2E, 12, 14 and 31. A significant number of analysis has been made including conventional (plugs and whole diameter) and special rock-core measurements and analysis (capillary pressure by centrifuge, porous plate and mercury injection, relative permeability, compressibility, electrical properties, wettability, nuclear magnetic resonance, etc). Figure 2.3 shows a cross-plot of permeability (k, mD) versus porosity (Φ, %), including parametric curves of constant k/Φ ratios to identify petrofacies. The plot includes all existing cores (4).

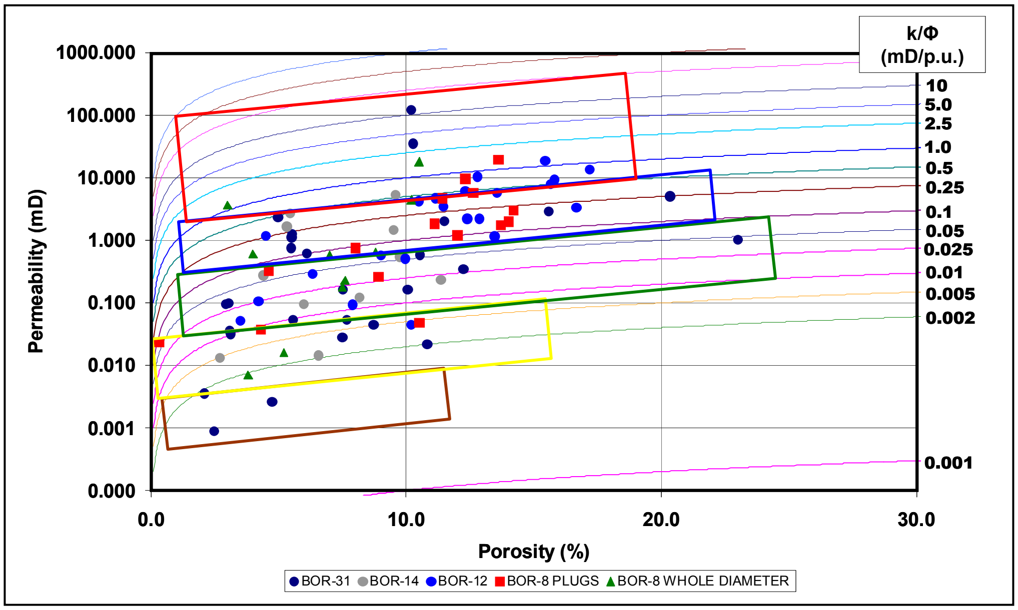

Figure 2.3. Permeability-porosity cross-plot including parametric curves of constant k/Φ for all existing cores. Triangular symbols represent conventional measurements performed on whole-diameter samples.

In addition, other geological analyses were made to obtain a better understanding of the heterogeneity in the lithology of "O BOR 2E" reservoir. They include detailed core descriptions, X-Ray diffraction analysis (XRD), scanning electron microscopy (SEM) analysis and detailed thin section petrography. Petrographic analyses were performed to address the following objectives: characterization of the fabric, texture, and mineralogy; determination of the types and patterns of cementation and diagenesis, and evaluation of reservoir quality.

2.4 SEDIMENTARY MODEL

Facies in “O BOR 2E” reservoir are sandstone, mixed sandstone-dolostone, dolostone, pelecypod limestone, foraminiferal limestone-siltstone and shale. Figure 2.4 shows results from sedimentological studies that describe these facies to represent deposition in a shallow-marine carbonate platform environment (Kupecz et al, 2000; Mendez, 2002). This model was also confirmed by a recent study (Omni-PDVSA, 2007), which describes that the carbonate sediments of the Escandalosa “O” Member consist predominantly of thin to thick bedded dolostones that were originally deposited as grain-rich to mud-rich limestone (e.g., skeletal grainstone and packstone, peloidal packstone and wackestone) on a shallow shelf. The amount of each facies varies depending on the zone across the field. One of the most important observations is that the best oil-producing wells are located in zones with large amounts of dolomite and with an increase in secondary porosity (interconnected vugs and fractures).

Figure 2.5 shows the stratigraphic column for the “O BOR-2E” reservoir of the Cenomanian-Turonian Escandalosa Formation (Kupecz et al., 2000).

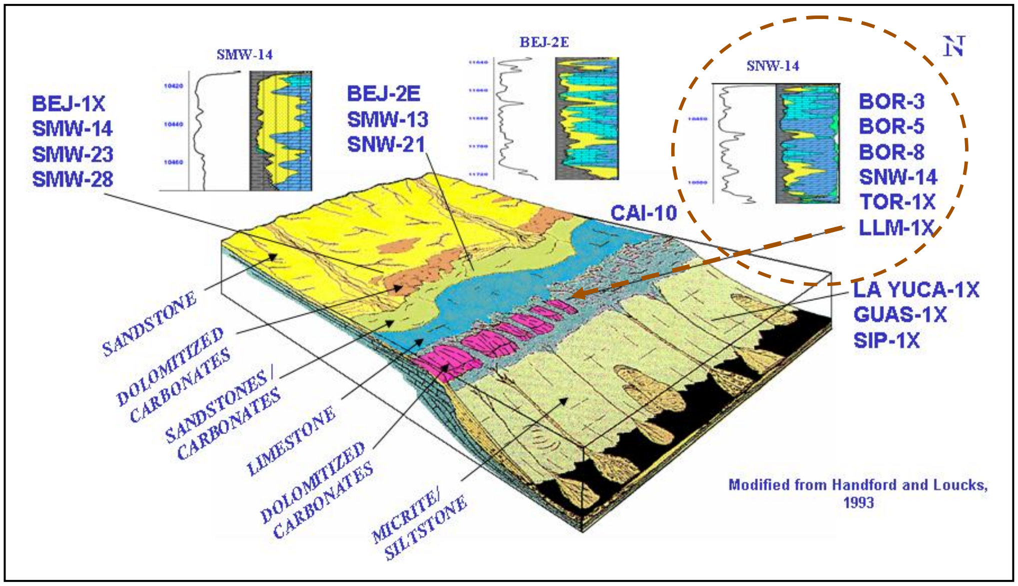

Modified from Handford and Loucks, 1993

Figure 2.4. Depositional Model for the "O" Member, Escandalosa Formation (excerpted from Mendez, 2002).

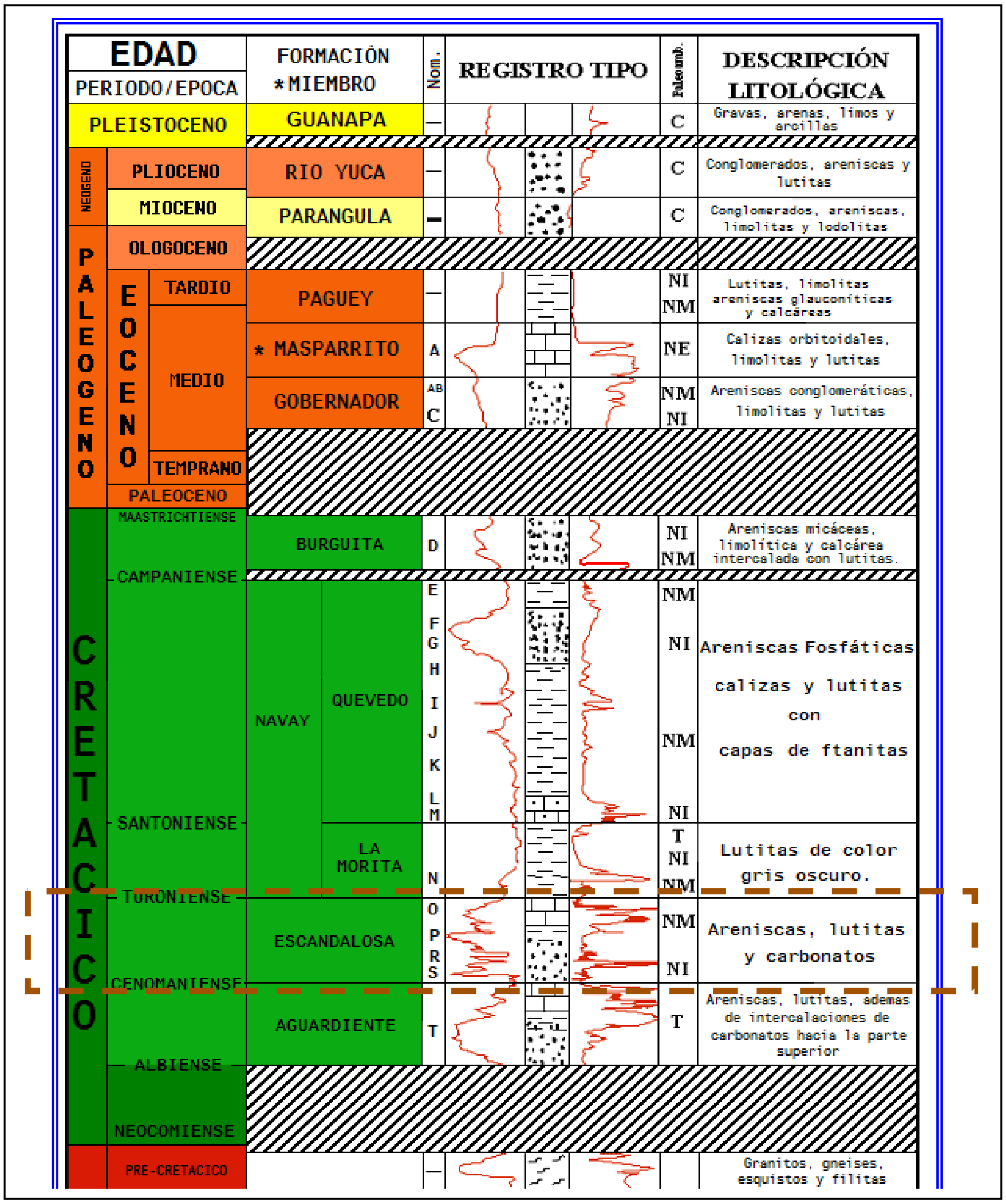

Figure 2.5. Stratigraphic column of the Barinas area showing the vertical location of the interval of interest (excerpted from PDVSA Internal Report, 2002).

2.5 PRESSURE TRANSIENT MEASUREMENTS

Pressure transient tests were acquired in "O BOR 2E" reservoir since the beginning of its production. These types of tests include build-up (BOR-2E and 12) and multi rate (BOR-8). In addition, there are pressure measurements obtained from static fluid levels, static gradients, pressure sensors located in the electrical submersible pumps (ESP) intake and formation testers. In this section, we only consider the results obtained in the build-up and multi-rate tests.

The first build-up test was performed in November 1994 in the well BOR-2E. It was kept flowing for one hour and then closed for a period of eight hours to obtain initial reservoir pressure. According to a PDVSA Internal Report (2003), the model used included storage and skin, double porosity and permeability and one fault to obtain a match between test and field data. An initial reservoir pressure of 4554 psia @ datum (11100 ft) was obtained with the model used. Results also included a permeability of **30 mD** for the whole system (matrix, vugs and fractures) and a fault located at a distance of 110 ft from well BOR-2E, among other variables. Figure 2.6 shows a log-log plot of the build-up test acquired in the well BOR-2E displaying a deflection of the derivative that indicates presence of a double porosity system.

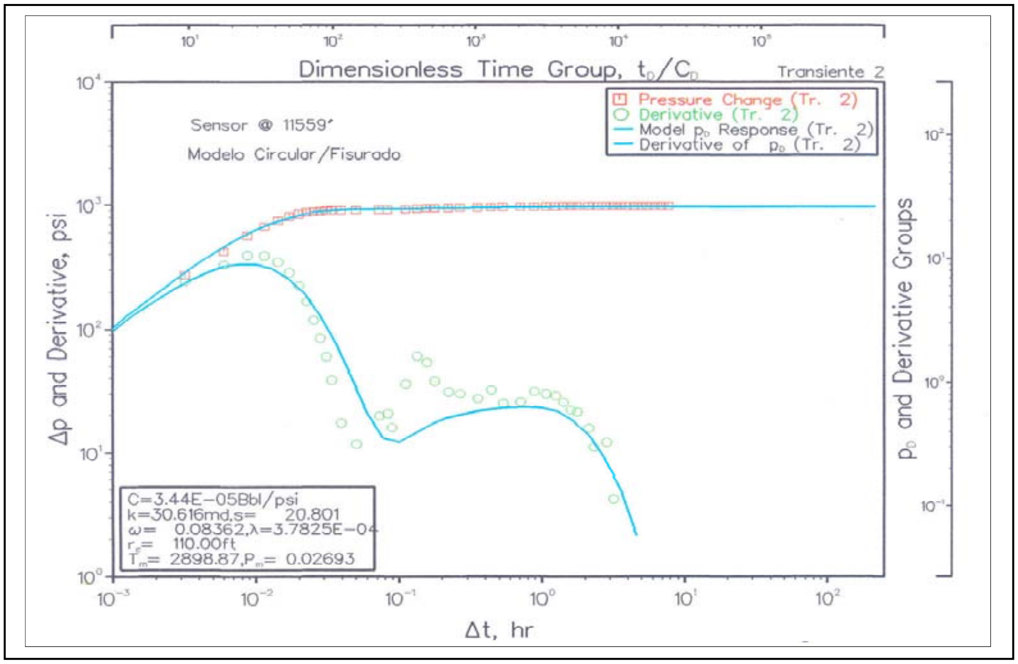

Figure 2.6. Log-log plot of the build-up test acquired in the well BOR-2E showing a deflection of the derivative that would be associated with the presence of a double porosity system (excerpted from PDVSA Internal Report, 2003).

Three years later, in 1997, a multi-rate test was acquired in the well BOR-8 that consisted in three flow periods and two build-up periods. Interpretation results were obtained from the second build-up period for being the one with largest duration (25 hours). For this test, the same model of the previous well was used (PDVSA internal report, 2003). The test had a radius of investigation of 5640 ft, with a reservoir pressure of 4215 psia @ datum. Permeability estimated for the whole system of **659 mD** with a fault at 1000 ft from the well. Figure 2.7 shows a log-log plot of the build-up test acquired in the well BOR-8.

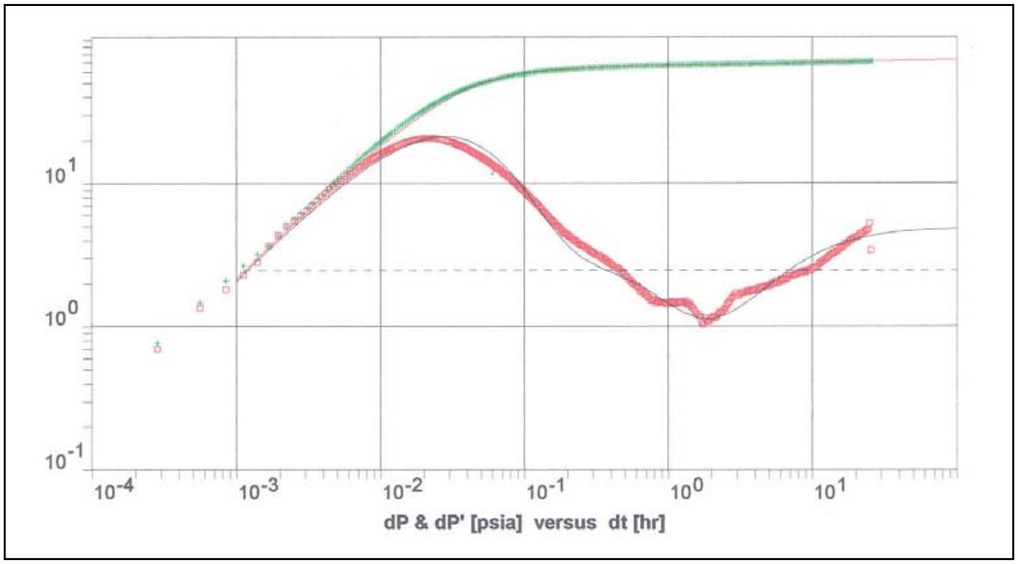

Figure 2.7. Log-log plot of the multi-rate test acquired in the well BOR-8 (excerpted from PDVSA Internal Report, 2003).

The last pressure transient test performed in the reservoir was a build-up test in the well BOR-12 (February, 2001). This test was performed with an ESP in the bottom of the well and results were obtained in real time with a sensor located in the pump intake. The model implemented for test interpretation considered storage and skin, double porosity and permeability with intersecting faults (60°). The test had a radius of investigation of 2080 ft, with a reservoir pressure of 2722 psia @ datum, permeability for the whole system of **101 mD** and a distance to each fault of 829 ft and 1250 ft. Figure 2.8 shows a log-log plot of the build-up test acquired in the well BOR-12.

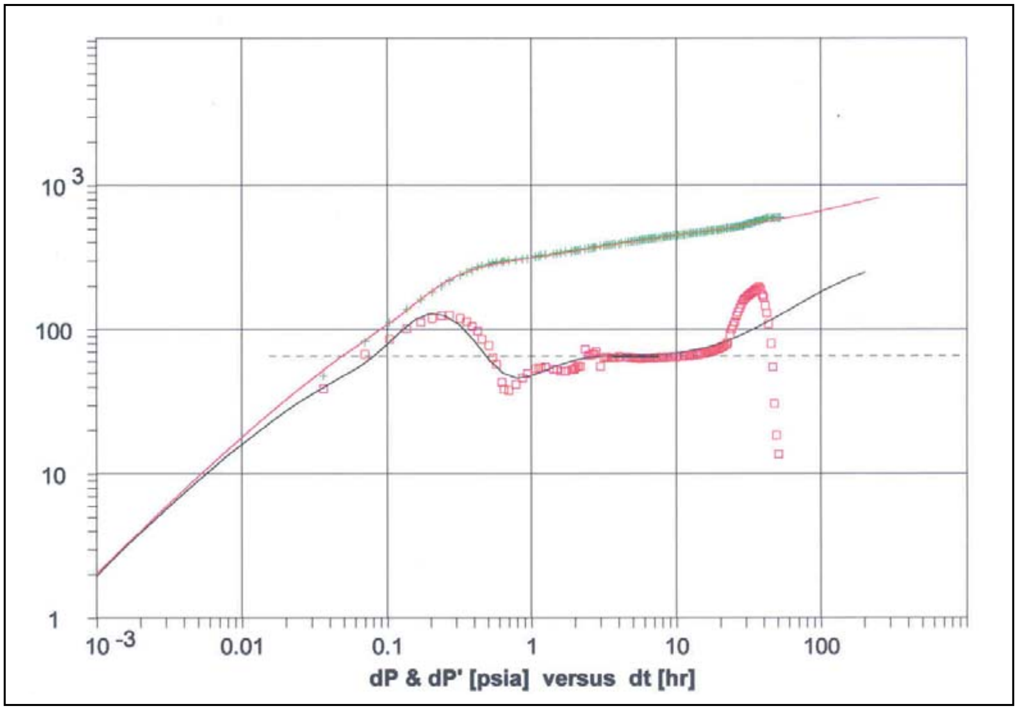

Figure 2.8. Log-log plot of the build-up test performed in the well BOR-12 (excerpted from PDVSA Internal Report, 2003).

2.6 PRODUCTION BEHAVIOR

Borburata field has 36 drilled wells with 20 wells that have produced in the reservoir “O BOR2E.” Currently, only 10 of them are still active mainly due to the decreasing reservoir pressure. Figure 2.9 displays the production behavior for each well with BOR-11 as the best producing well from this reservoir. Most of the changes in oil production are because of variations of the water-cut and pressure decline associated with production.

The oil gravity is 28 with a variable water-cut that varies depending on the reservoir area where the well was drilled. There are three types of water-cut behavior: a) those wells that started with a low water-cut and have kept their water-cut with time; b) those that started with a low water-cut and then increased with time; c) those that started with relatively high water-cut and have maintained without changes. Figure 2.10 describes the water-cut behavior.

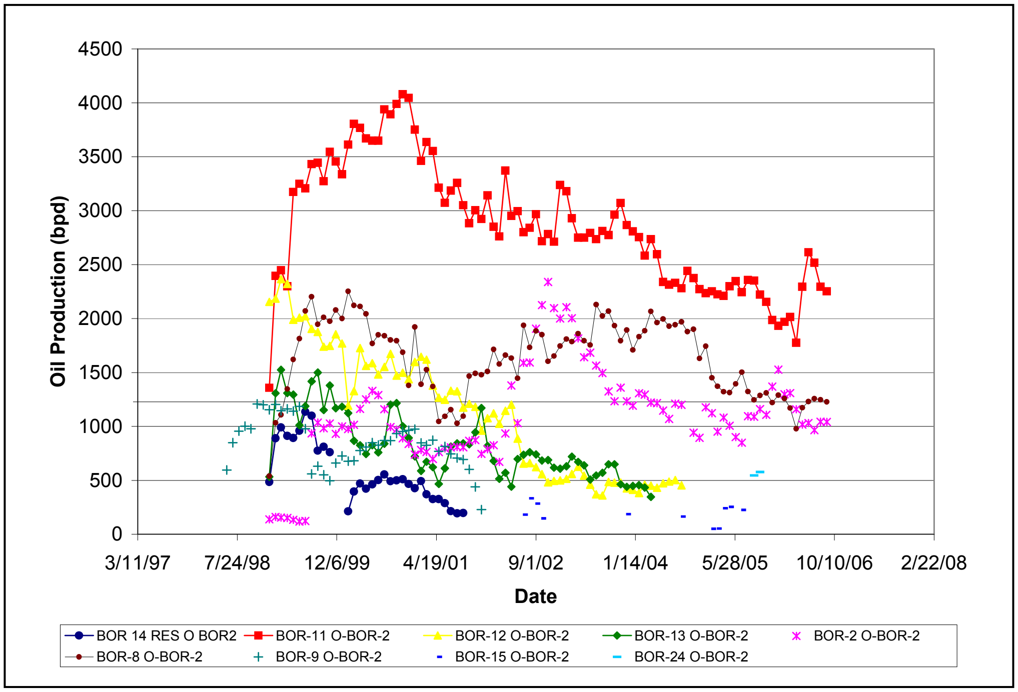

Figure 2.9. Production behavior for each well that has produced in the reservoir "O BOR-2E" showing a wide range of production rates (original data obtained from PDVSA).

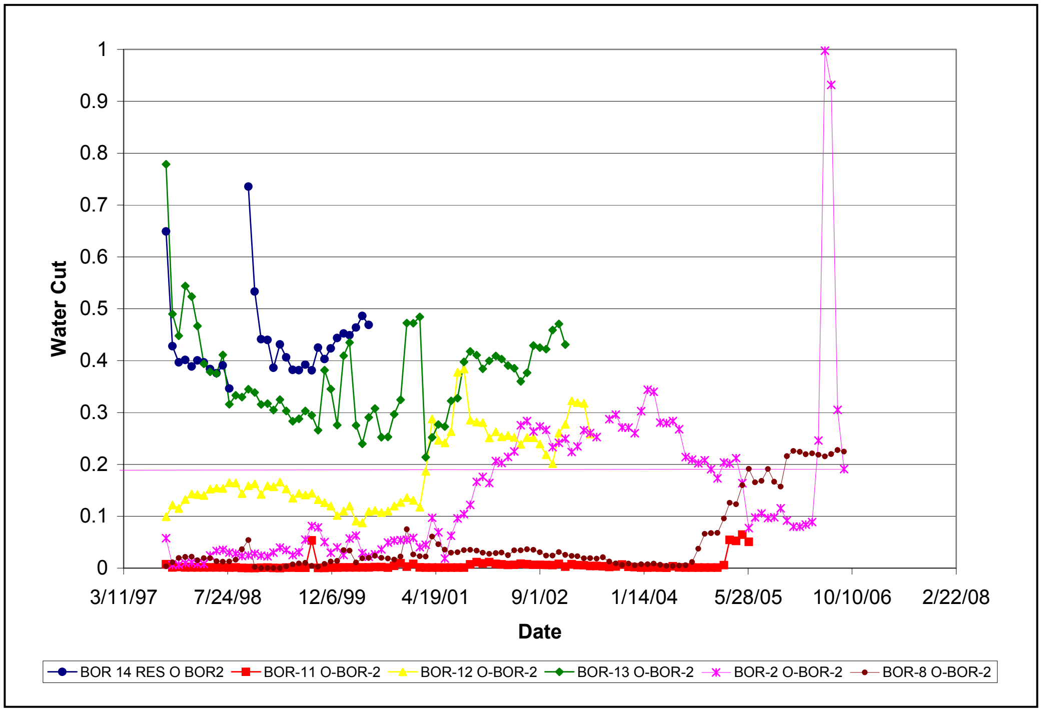

Figure 2.10. Water-cut behavior for each well that has produced in the reservoir "O BOR-2E" showing three types of water-cut behavior (Original data obtained from PDVSA).

Finally, Figure 2.11 shows a structural map of the main area of this reservoir with all the information described earlier.

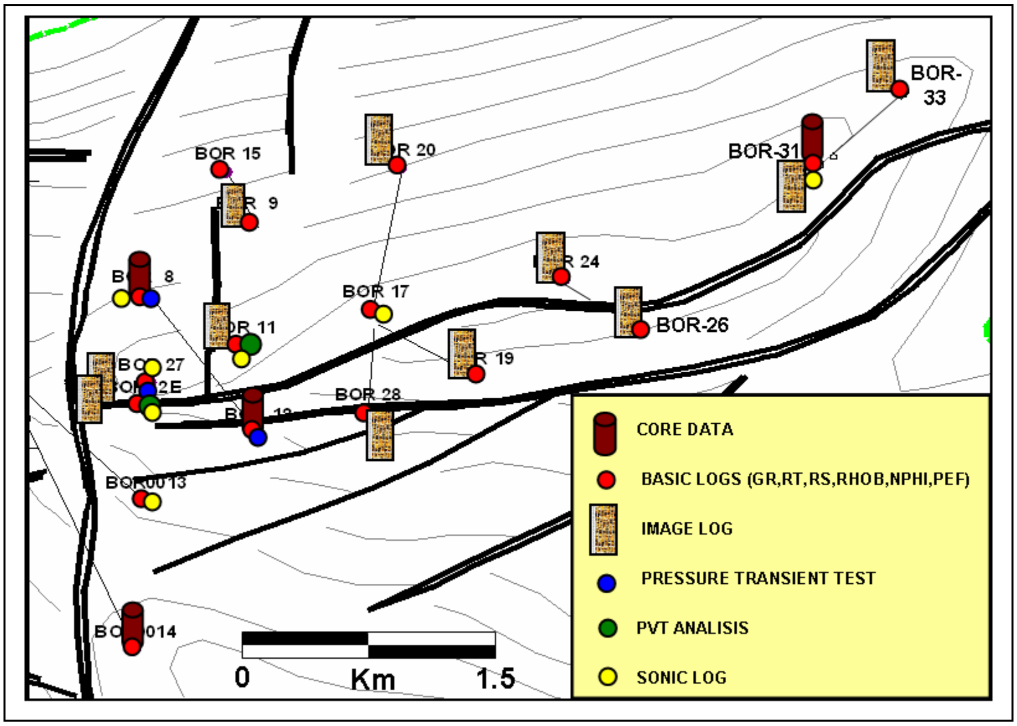

Figure 2.11. Structural Map of the main area of the reservoir showing the most important information for each well in the Borburata field.

CHAPTER 3

Petrophysical Assessment

This chapter describes the petrographic analysis of the reservoir under consideration which includes the sedimentological model together with facies and mineralogy analysis. Additionally, we describe petrophysical properties and the method used for rock typing based on Winland's approach (Pittman, 1992). Lucia's method (Lucia, 1995; Jennings and Lucia, 2003) was also implemented with rock-core measurements combined with thin sections and sedimentological descriptions. Finally, we describe the equations and procedure implemented for petrophysical assessment.

3.1 PETROGRAPHIC ANALYSIS

The sedimentological study performed on rock-core samples indicates presence of the following facies: sandstone, mixed sandstone-dolostone, dolostone, pelecypod limestone, foraminiferal limestone-siltstone, and shale. Facies distribution varies vertically as observed in Figure 3.1 and also varies along the reservoir area. Figure 3.1 additionally shows an interval where massive dolomitization took place based on the interpretation of core data. Sin-sedimentary and diagenetic fractures are also observed as well as high density of vugs with large variety of sizes (micro to megavugs). The main porosity on this interval is due to the system of vugs which are also connected to the rest of the porosity provided by matrix and fractures. In addition, it was determined that a high dolomitization process derived from an arid tidal flat (sabkha) environment took place in the interval analyzed. The latter is the main flow unit in the well with facies including intercrystalline, intracrystalline, moldic and vuggy porosity (12840'), as shown in the thin sections of Figure 3.2. The diameter of the vugs varies from millimeters to centimeters. Most of the oil is stored in the type of porosity produced by the communication of intercrystalline and intracrystalline porosity and fractures, according to previous sedimentological studies (Mendez, 2002; Kupecz et al., 2000). The previous observations also apply to other wells (BOR-14 and 8) located in the same part of the reservoir.

Earlier sedimentological studies describe previously presented facies to represent deposition in a shallow-marine carbonate platform environment, indicating that the carbonate sediments of the Escandalosa "O" Member consist predominantly of thin to thick bedded dolostones that were originally deposited as grain-rich to mud-rich limestone (e.g., skeletal grainstone and packstone, peloidal packstone and wackestone) on a shallow shelf. The distribution of each facies varies depending not only on the zone across the field but also on the vertical section of the reservoir.

In addition, the carbonate reservoir is considered a triple-porosity petrophysical system (matrix + vugs + fractures), according to observations and analysis of rock-core measurements, non-conventional well-log data and pressure transient measurements.

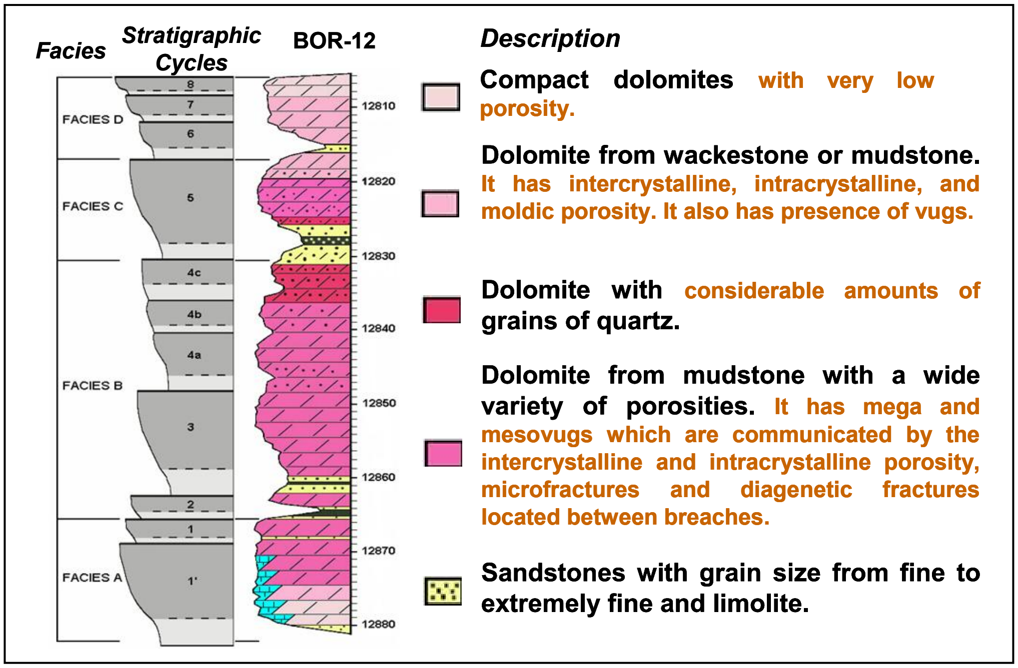

Figure 3.1. Sedimentological Description of Well BOR-12 showing the typical mineralogy of the matrix of the "O BOR 2E" reservoir (modified from Mendez, 2002).

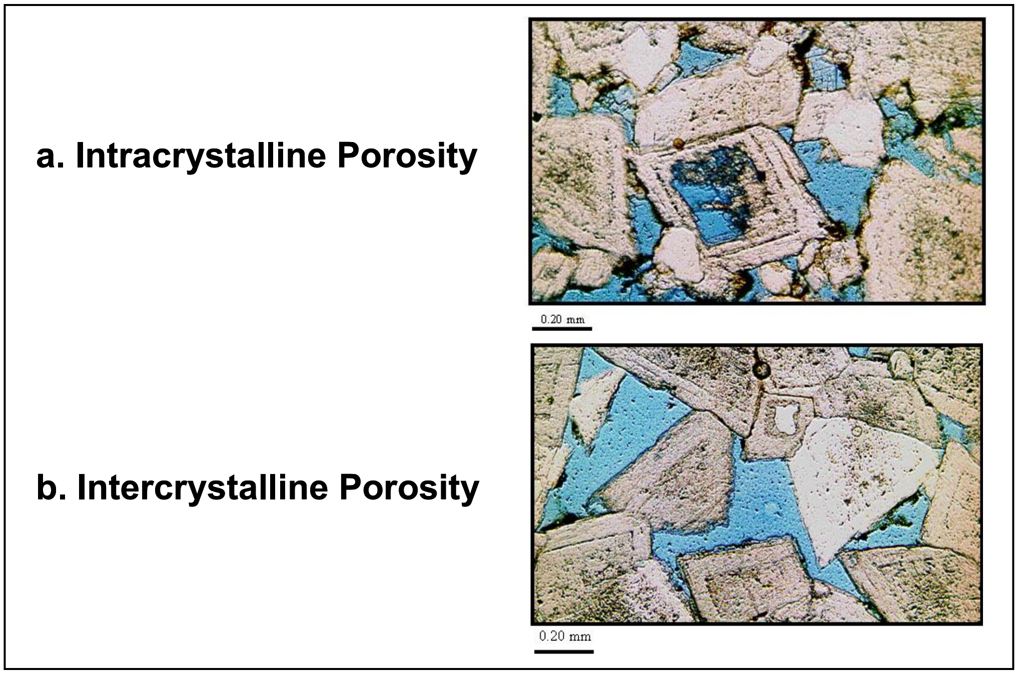

Figure 3.2. Thin sections obtained from rock-core data of Well BOR-12 showing: (a) intracrystalline or separate-vug porosity and (b) intercrystalline porosity that contributes to the increase in the total porosity and permeability of the petrophysical system. Moldic and vuggy porosity were also observed in this interval but it is not shown due to the size of the thin section.

3.2 PETROPHYSICAL CHARACTERISTICS AND ROCK TYPING

We applied the Winland approach (Pittman, 1992) to characterize the different types of reservoir rocks of the “O BOR 2E” reservoir using mercury injection capillary-pressure data. To apply Winland’s method, we used the rock-core measurements described in Figure 3.3, where we emphasize the available mercury injection capillary-pressure data. The cross-plot of permeability (k, mD) versus porosity (ϕ, %) displays parametric curves for constant k/ϕ ratios used to identify rock types. We observe four rocks types identified with color boxes. Pore throat radius (r, μm) is estimated from mercury injection capillary-pressure data applying the equation

$$r = \frac{2\sigma\cos\theta}{P_C}, \tag{3.1}$$

where σ (dynes/cm) is the interfacial tension, θ (deg) is the contact angle between the fluid interface and the rock and P_C (psi) is the capillary pressure obtained from mercury injection rock-core measurements. The values of σ and θ for an air-mercury system, are 480 dynes/cm and 140°, respectively (Tiab and Donaldson, 2004).

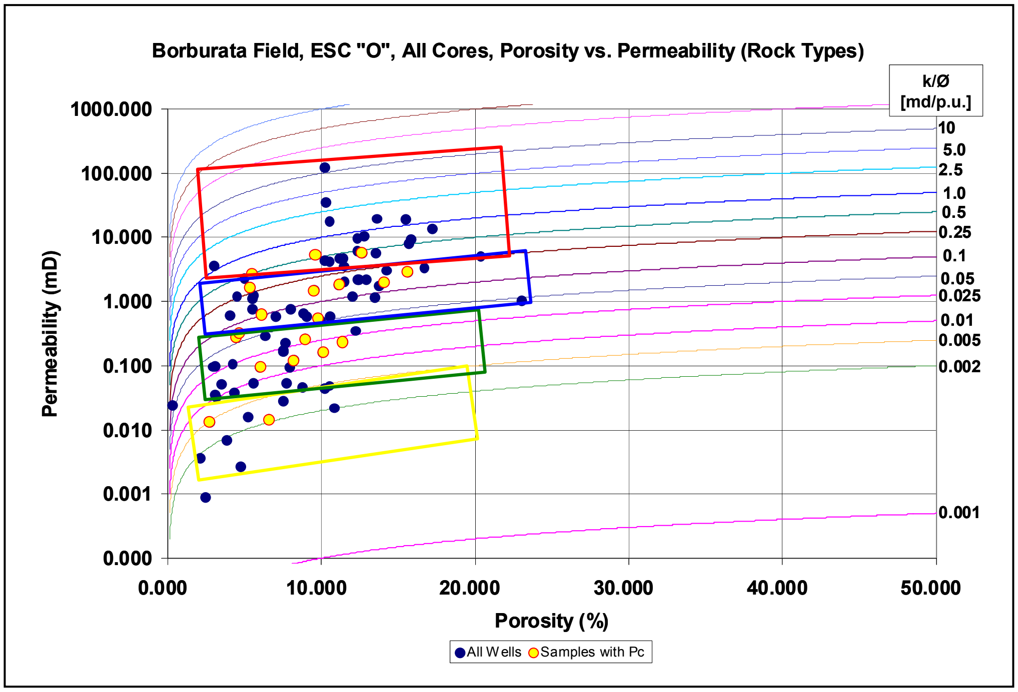

Figure 3.3. Porosity-permeability cross-plot displaying parametric curves of constant k/Ø ratios. The parametric curves indicate presence of four main rock types (large triangles). Yellow circles represent those samples with capillary pressure measurements.

Pore throat radius can be estimated from Winland’s method

$$Log(r_{35}) = 0.732 + 0.588 * Log(k_{air}) - 0.864 * Log(\phi) \qquad (3.2)$$

where r_{35} (µm) is pore-aperture radius corresponding to the 35th mercury-saturation percentile, k (mD) is uncorrected air permeability, and ϕ (%) is porosity. Figure 3.4 shows the pore throat radius parametric curves obtained after applying the above equation. The plot is a porosity-permeability cross-plot that includes parametric curves of Winland’s critical pore-throat radius, R35 and constant k/Ø ratios.

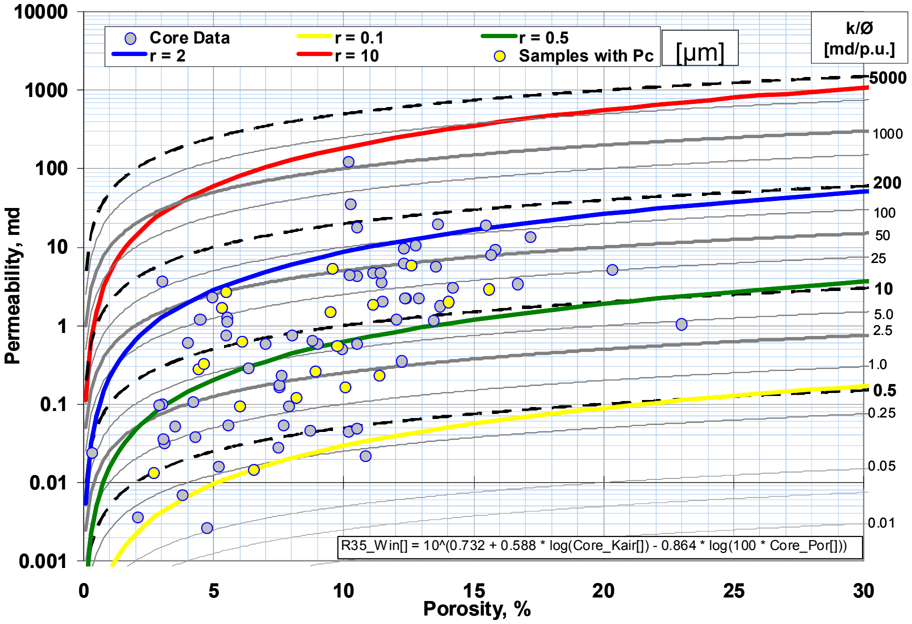

Figure 3.4. Porosity-permeability cross-plot displaying parametric curves of Winland’s critical pore-throat radius, R35 (continuous colored lines) and constant k/Ø ratios (grey-continuous and dashed-black lines). Parametric curves indicate presence of four main rock types: (1) Samples with Winland’s critical pore-throat radius, R35 (r), less than 0.1 µm; (2) Samples with r between 0.1 µm and 0.5 µm; (3) Samples with r between 0.5 µm and 2 µm; (4) Samples with r between 2 µm and 10 µm. Yellow circles identify samples with capillary pressure measurements.

Figure 3.5 shows the mercury injection capillary-pressure data used to implement Winland's method. Four different rock types are identified in this plot where yellow lines identify the worst type of rock (highest displacement pressure) and red lines identify the best type of rock (lowest displacement pressure). Green and blue lines identify intermediate-quality rocks.

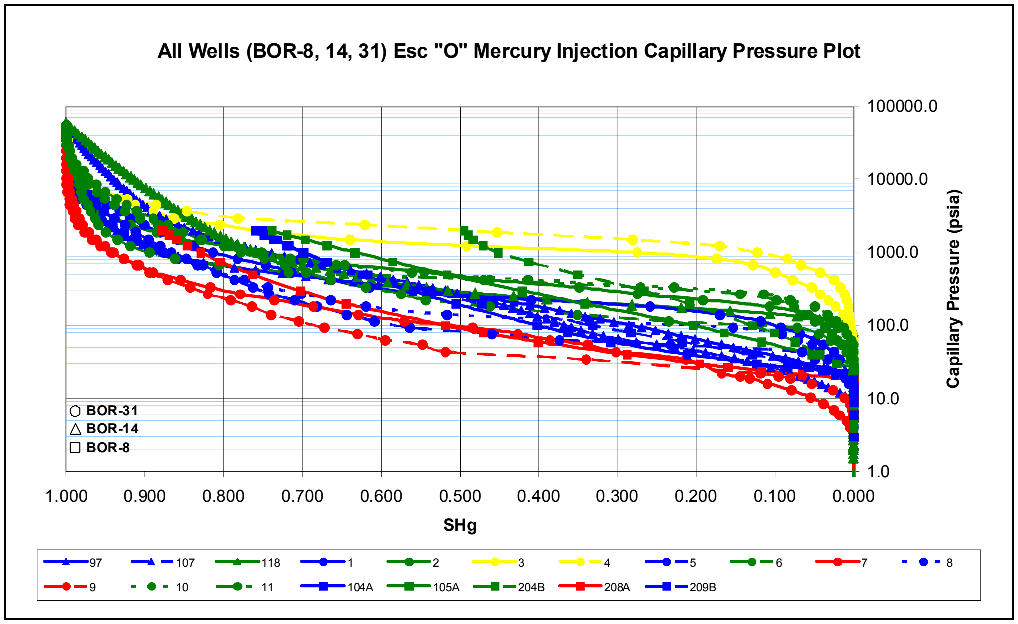

Figure 3.5. Mercury injection capillary-pressure data. Capillary pressure curves indicate presence of four main rock types.

Additionally, we plotted incremental mercury saturation versus pore-throat radius (equation 3.1) to identify rock types. Figure 3.6 shows the corresponding results. The incremental mercury saturation plot indicates the dominant pore-throat aperture and rock type at the maximum of each curve. We used rock-core measurements from three different wells. However, incremental mercury saturation curves indicate presence of four main rock types.

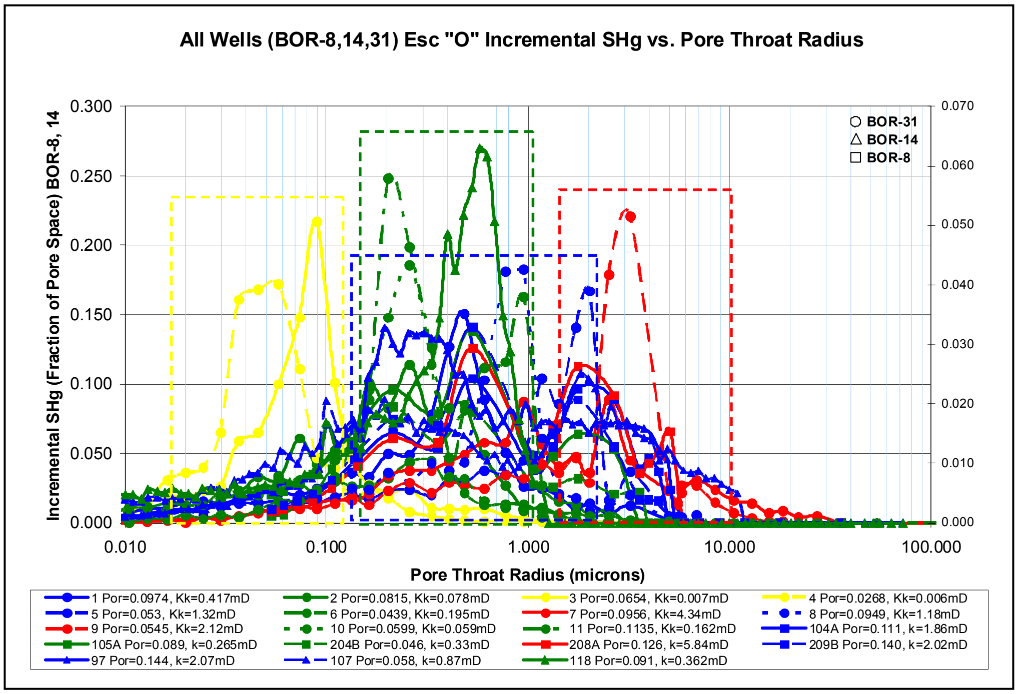

Figure 3.6. Incremental mercury saturation plot obtained from mercury injection capillary-pressure measurements. Dominant pore-throat aperture and rock type are indicated by the maximum of each curve. The curves indicate presence of four main rock types (dashed-color boxes).

We also applied Lucia's method (Lucia, 1995; Jennings and Lucia, 2003) based on rock-core measurements combined with thin sections and sedimentological descriptions. This step enabled us to improve the calculation of initial values of petrophysical properties.

Figure 3.7 shows a porosity-permeability cross-plot with samples classified by rock fabric and based on predictions from the generalized porosity/permeability/rock-fabric model (Jennings and Lucia, 2003), displaying parametric curves of constant k/Ø ratios as well. We identified three different rock fabrics. However, a group of samples with low permeability and porosity values appeared as a fourth rock fabric having the lowest porosity and permeability values. We were not able to confirm whether these samples corresponded to bad-quality laboratory measurements.

Finally, Figure 3.8 compares porosity-permeability cross-plots with samples classified by rock fabric to predictions from the generalized porosity/permeability/rock-fabric model, parametric curves of Winland's critical pore-throat radius, R35 and constant k/Ø ratios. We observe uniform pore sizes across the rock-fabric fields from the comparison of this rock-fabric classification to the cross-plot of porosity, permeability and R35 pore size. According to Lucia (1999), pore size varies within depositional rock-fabric classes. As a result, uniform pore size is not the fundamental link between petrophysical properties and depositional or dolomite facies. Lucia emphasizes that the fundamental link is through rock fabrics. We have already observed the large variability in petrophysical properties present in carbonate reservoirs. This characteristic is even more remarkable in permeability. Because permeability is highly linked to R35 pore size, we can conclude that R35 is highly variable as well. Therefore, there is no need to assume that a depositional facies can be characterized by a uniform pore size. It is also important to highlight that the R35 approach cannot be applied to vuggy carbonate reservoirs.

On the other hand, Martin et al. (1999) and Lucia (1995) explained that pore-throat size is reflected by rock fabric, which is the consequence of deposition and diagenesis. As a result, similar k/ϕ ratios or R35 of a population of samples provide the means to subdividing a depositional cycle into flow units. Lucia's technique (1995) has a significant value in the description of reservoirs where outcrop and core measurements are physically available for detailed study of events and features, visual description of porosity through thin sections, and sampling for additional core analysis and modeling. The application of this technique to carbonate reservoirs with more limited data sets such as the one considered in this thesis, presence of large crystal dolostones (>100 μm), and presence of large touching vugs is more constraining. Figure 3.9 is a detailed description of Lucia's petrophysical classification method for carbonate reservoirs. We already defined three or even four rock-fabrics from the plot of Figure 3.7. However, when we apply Lucia's classification (1995) to thin sections obtained in the key well (Figure 3.10), we concluded that there exists only one petrophysical class: Class 1, large crystalline (average about 300 μm) dolostones.

Through the analysis of thin sections, we observe that only two samples have significant visible pore space. The sample at 11682 ft exhibits a considerable number of rounded separate vugs of unknown origin and some intercrystalline porosity, whereas the sample at 11715 ft has a considerable intercrystalline porosity but silt-sized quartz grains fill much of the intercrystalline pore space. In addition, SEM photos shown in Figure 3.11 and the X-ray analysis indicate presence of clay minerals. These three factors tend to reduce permeability. Only four of the six thin sections have porosity and permeability rock-core measurements and only three have more than 0.1 mD permeability, which is a small sample for analysis. In general, porosity and permeability rock-core measurements are spread from the petrophysical class 1 field to the class 3 field; although thin sections are all class 1 large crystalline dolostones. The one thin section that plots in the class 1 field exhibits hairline fractures and the two samples that plot in the class 3 field are silty with separate vugs.

According to the sedimentological description of the core acquired in well BOR-31 (Omni, 2007), the lithology of samples without thin sections is heterogeneous with a mineralogy distribution that varies along the entire reservoir. There is a mixture of carbonate, siliciclastics and clay minerals in such samples. Thin sections of all the data points are required for rock fabric analysis before any conclusions can be made as to the relationship between fabric and petrophysical properties for these samples.

We believe that a combination of the previous two approaches would enable a better reservoir characterization of the matrix due to the amount and low variety of thin sections and rock-core measurements available.

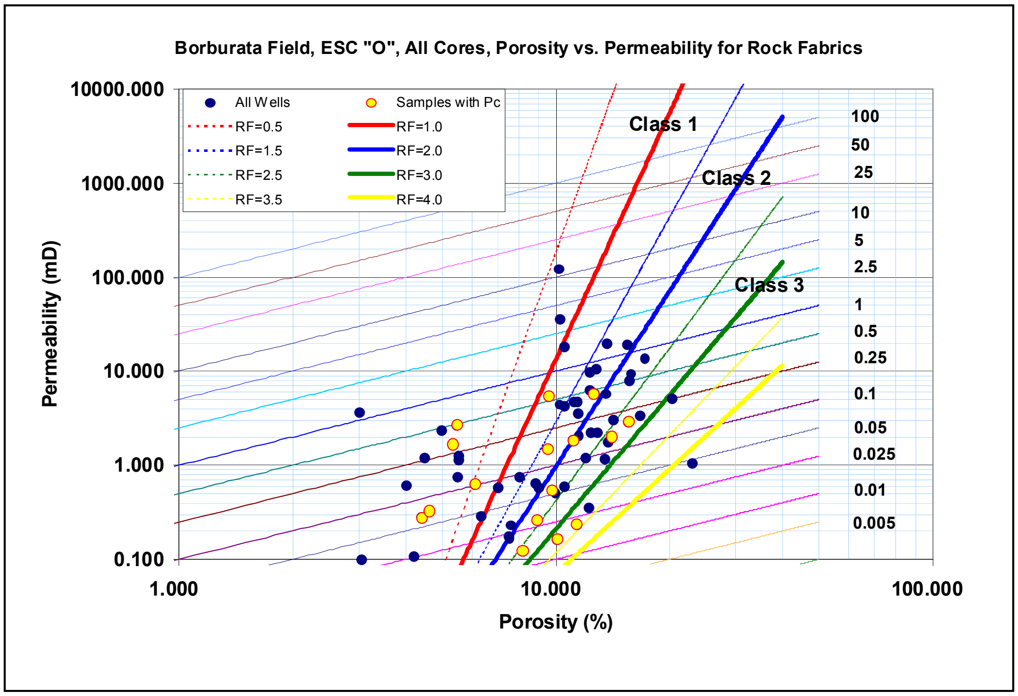

Figure 3.7. Porosity-permeability cross-plot of samples classified by rock fabric and based on predictions from the generalized porosity/permeability/rock-fabric model (color-thick lines) displaying parametric curves of constant k/Ø ratios (color-thin lines). The plot considers three rock fabrics. However, a group of samples with low values of permeability and porosity appear as a fourth rock fabric in the left and lower part of the cross plot. Yellow circles identify samples with capillary pressure measurements.

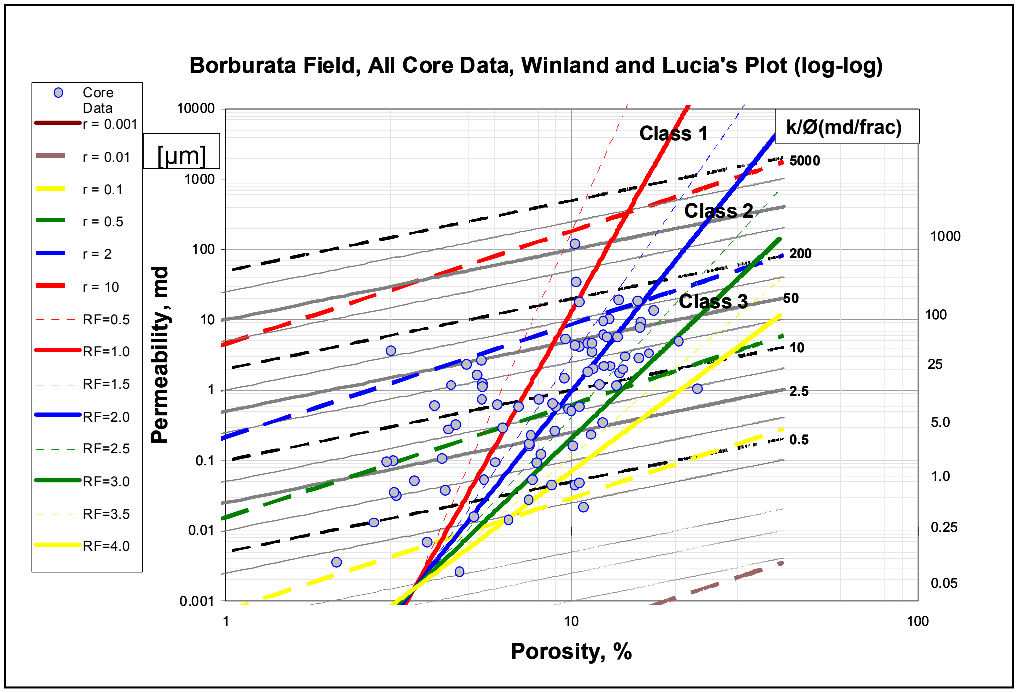

Figure 3.8. Porosity-permeability cross-plot with samples classified by rock fabric and based on predictions from the generalized porosity/permeability/rock-fabric model (continuous-colored thick lines) with parametric curves of Winland's critical pore-throat radius, R35 (dashed-colored lines) and constant k/Ø ratios (grey-continuous and dashed-black lines).

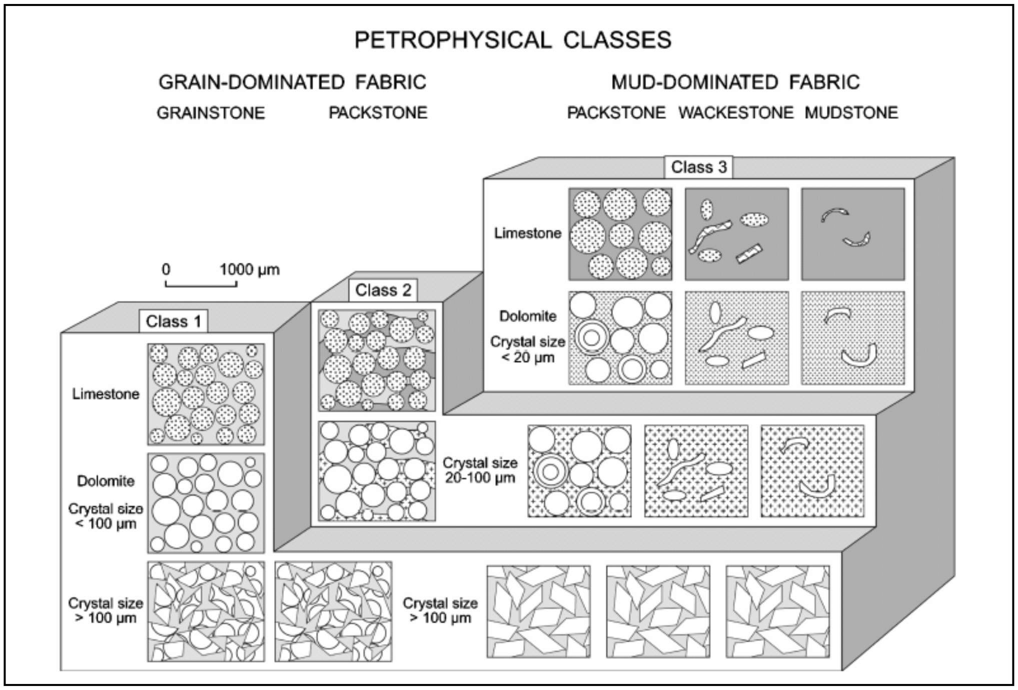

Figure 3.9. Lucia's (1995) petrophysical classification for carbonate reservoirs. The classification is based on rock-fabric petrophysical classes grouping particle size and sorting fabrics with similar interparticle porosity/permeability relationships (excerpted from Lucia, 1995).

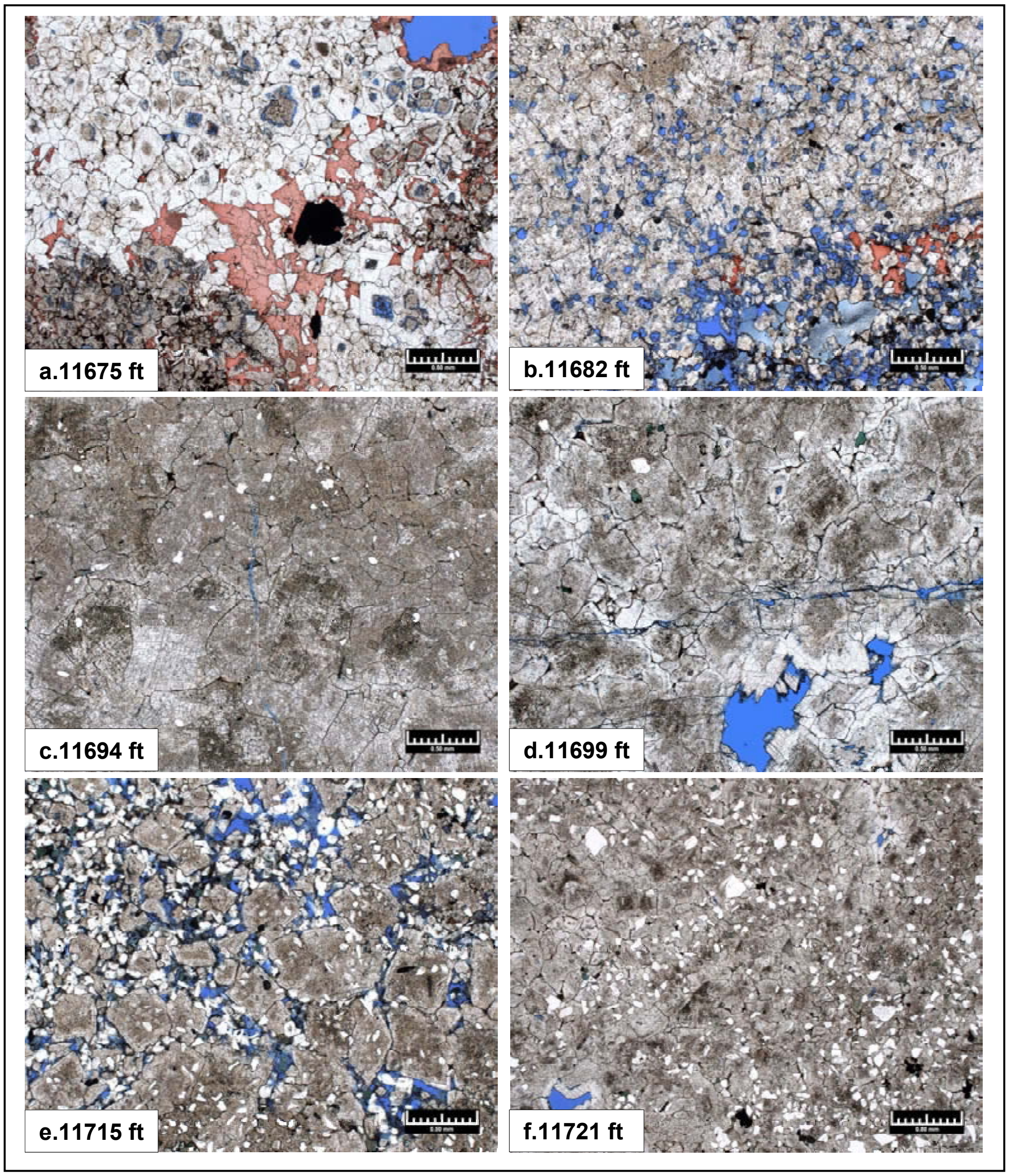

Figure 3.10. Photomicrographs taken of thin sections acquired in the key well (BOR-31). The samples show only one rock-fabric class: large crystal dolostones (average size equal to 300 μm).

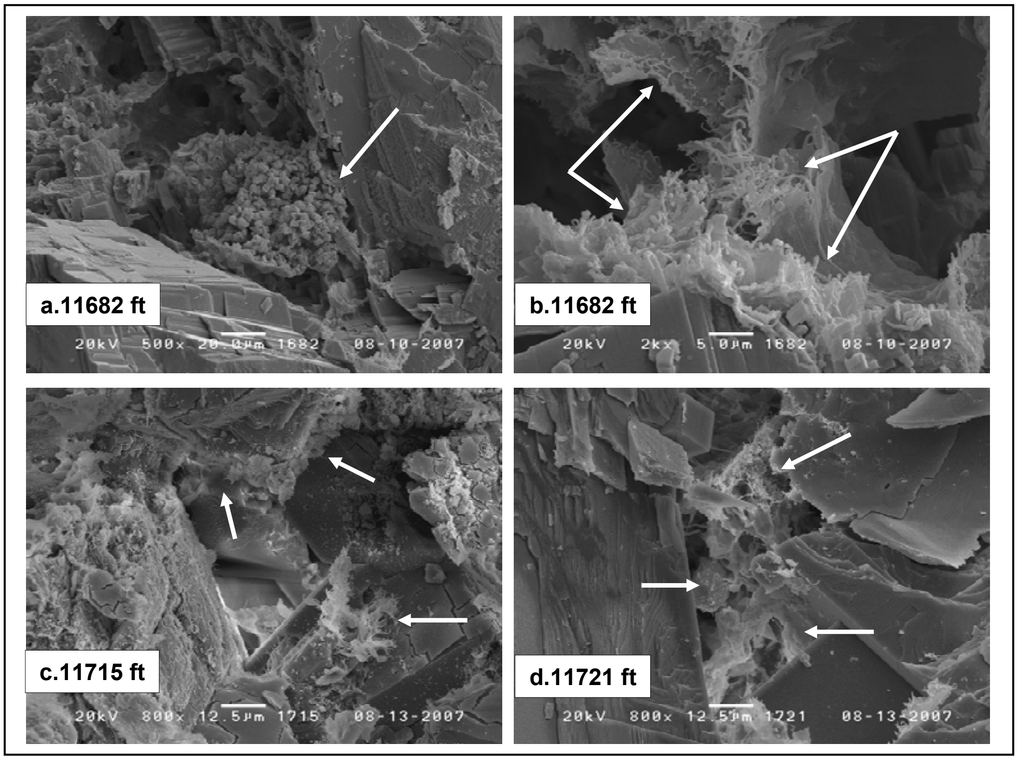

Figure 3.11. SEM photos taken from the core acquired in the key well (BOR-31). The samples show presence of clay minerals that reduce the petrophysical quality of the rock causing some of the heterogeneity observed in porosity-permeability cross-plots. White arrows indicate clay minerals deposited around the pore throats or else occluding them.

3.3 MULTI-MINERAL APPROACH

To perform the petrophysical assessment, we implemented a multi-mineral approach because of the presence of several minerals components along the depth interval of interest. These minerals components are sandstone (SS), dolostone (DS), limestone (LS), a mixture of sandstone and dolostone (SS+DS), and shale (Sh).

We worked with an inverse and forward solution to approach the multi-mineral petrophysical description. The response of well logs is combined with the response parameters for each component to estimate mineral and fluid volumes in the pore space. The model enables a material balance of all the components defined during the input process, namely

$$V_{DS} + V_{SS} + V_{LS} + V_{Sh} + \phi = 1, \tag{3.3}$$

where V_{DS} is the volume of dolomite, V_{SS} is the volume of sandstone, V_{LS} is the volume of limestone, V_{Sh} is the volume of shale and ϕ is the porosity of the rock.

We used the available well logs in each well to define the input model. The model then assumes that each well log measurement is the result of total sum of the individual contributions of each component. At the same time, each well log has a weight depending on the characteristics of the measurement and offers corresponding uncertainty.

For instance, the formation density (ρ_b) and each one of the parameters that we considered for the total response of the log is given by

$$\rho_b = V_{DS} * \rho_{bDS} + V_{LS} * \rho_{bLS} + V_{SS} * \rho_{bSS} + V_{sh} * \rho_{bSh} + \phi * \rho_{bF} \tag{3.4}$$

where ρ_b is the reading of density log, V_{DS} is the volume of dolomite, ρ_{bDS} is the reading of density log of dolomite, V_{LS} is the volume of limestone, ρ_{bLS} is the reading of density log of limestone, V_{SS} is the volume of sandstone, ρ_{bSS} is the reading of density log of sandstone, V_{sh} is the volumetric concentration of shale, ρ_{bSh} is the reading of density log of shale, ϕ is the porosity of the rock, and ρ_{bF} is the reading of density log of the fluid.

After performing the analysis in each well log we observe that the final result is a matrix (n+1*n+1), where n is the number of logs. We add the material balance equation previously described (3.3) to complete the system of equations and to find a solution for the volumetric concentration of each component.

The above approach was implemented in wells with rock-core measurements (X-ray analysis) to calibrate the mineralogy and the lithology obtained from well logs. Such cross-validation exercise enabled a good match with the mineralogy obtained from the rock-core measurements. Subsequently, we implemented the same approach to the remaining of the wells assuming the same lithology and mineralogy response of the key wells.

3.4 EFFECTIVE POROSITY AND WATER SATURATION FROM WELL LOGS

We used a combination of porosities from bulk density and neutron logs (Dewan, 1983) to estimate effective porosity (ϕ_e). First, well-log measurements were corrected for shale content as follows:

$$\phi_{DC} = \phi_D - C_{sh} * \phi_{Dsh} \text{, and} \tag{3.5}$$

$$\phi_{NC} = \phi_N - C_{sh} * \phi_{Nsh} \text{,} \tag{3.6}$$

where ϕ_{DC} is the porosity obtained from bulk density log corrected by content of shale, ϕ_D is the porosity obtained from bulk density log without corrections by content of shale, C_{sh} is the content of shale, ϕ_{Dsh} is the bulk density log response in a shale formation, ϕ_{NC} is the porosity obtained from neutron log corrected by content of shale, ϕ_N is the porosity obtained from neutron log without corrections by content of shale, and ϕ_{Nsh} is the neutron log response in a shale formation.

Since there is no gas present in the reservoir, the corrected porosity values should be close together. Effective porosity was estimated with

$$\phi_e = \frac{(\phi_{DC} + \phi_{NC})}{2} \tag{3.7}$$

where ϕ_e is effective porosity.

The first cores acquired in the reservoir do not contain rock-core water saturation measurements (BOR-8 and BOR-12). Those that do have such information were not drilled in the main area of the reservoir (BOR-5E) or acquired in the section of interest (BOR-2E). The most recent cores acquired in the reservoir were in wells BOR-14 and BOR-31. From rock-core measurements performed in the first well, water saturation fluctuates between 1 to 12% with grain densities from 2.16 to 2.87 gr/cc. In the second well, water saturation fluctuates between 24 to 72%, with grain densities from 2.61 to 2.88 gr/cc. In both cases, the wide variety of grain density values is due to presence of different facies along the vertical section. Both cores were acquired in WBM.

Water saturation (Sw) was computed from well-log measurements through Archie's equation (Archie, 1942) i.e.,

$$Sw = \sqrt[n]{\frac{a * R_w}{\phi^m * R_t}} \qquad (3.8)$$

Where a is tortuosity factor, R_w is connate water resistivity, ϕ is effective porosity, and m and n are the cementation and saturation exponents, respectively.

For "O BOR 2E" reservoir, we assumed values of 1.84 and 2 for the cementation and saturation exponents, respectively (Rangel, 2003). The tortuosity factor is taken as 1 in equation 3.8 based on the type of lithology already observed in the sedimentological description.

Connate-water resistivity at reservoir conditions was estimated using a salinity of 6700 ppm, whereupon R_w is equal to 0.23 Ohm-m at reservoir temperature. The Deep Laterolog Resistivity measurement, LLD, and High-Resolution Laterolog Array Tool, RLA5, are assumed as the true formation resistivity in the virgin zone. In this thesis we only applied our method in wells with resistivity measurements acquired in WBM.

3.5 ESTIMATION OF PERMEABILITY

In clastic reservoirs, it is common to estimate relationships between porosity and permeability measurements obtained from rock-core data and well logs in wells where both pieces of data are available. Subsequently, one extrapolates the relationship to estimate values of permeability in wells with no rock-core measurements. In carbonate reservoirs, it is difficult to find a straightforward relationship, largely because of the presence of other components (vugs and fractures) that modify the permeability of the system.

As it has been previously emphasized, the carbonate reservoir under consideration is a triple-porosity petrophysical system (matrix + vugs + fractures). Therefore, permeability values from rock-core measurements will most predominantly honor the permeability of the matrix and not the permeability of the entire petrophysical system.

Nonetheless, we initially estimate permeability using one of the published relationships (Jennings and Lucia, 2003). Subsequently, we assume that in those cases where there is no agreement with results obtained from the mud-filtrate invasion model that there is the presence of other components that affect the total porosity and permeability of the petrophysical system.

Finally, Figure 3.12 describes the petrophysical assessment in the key well (BOR-31). The results were obtained with the application of the previously described equations and parameters.

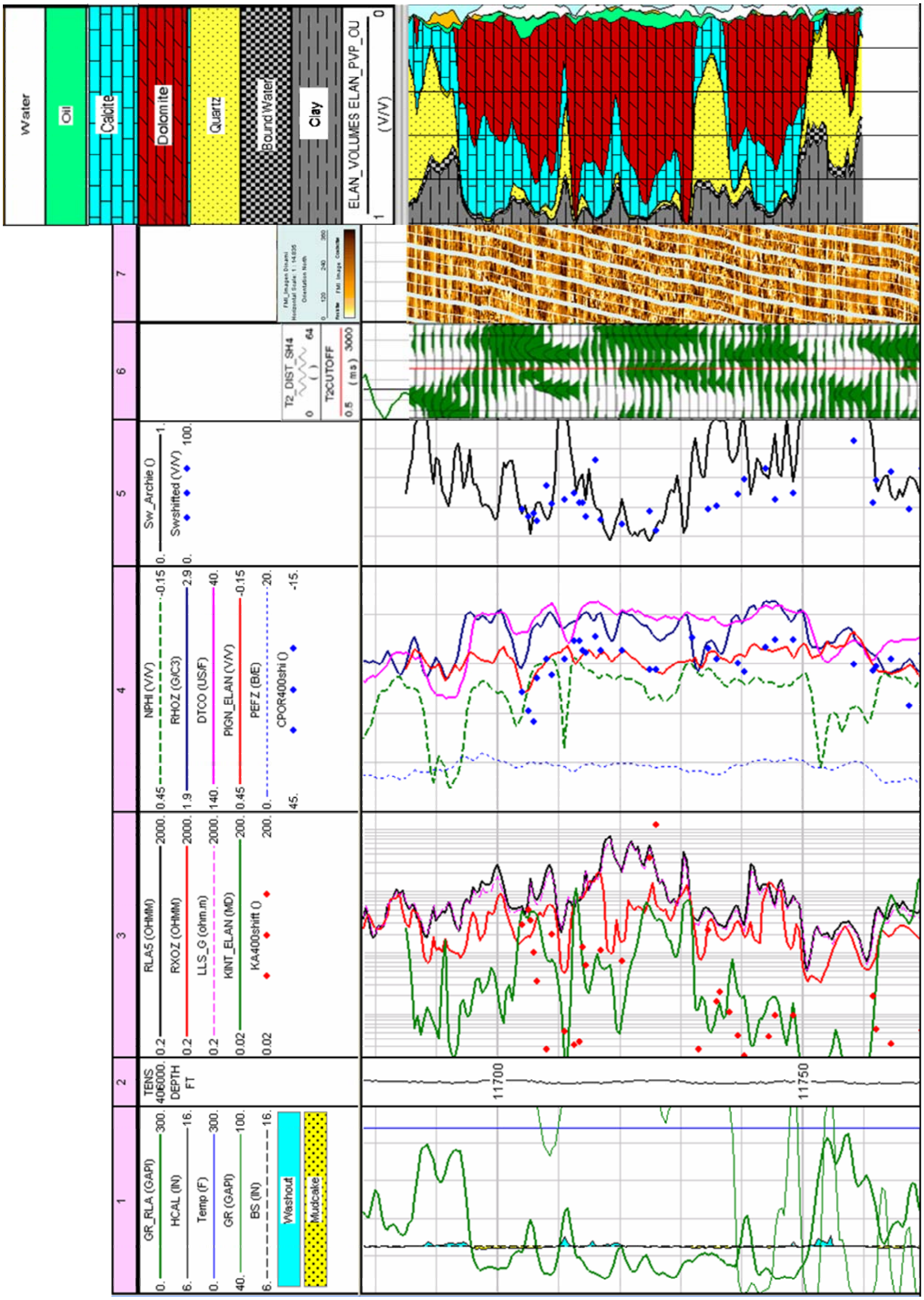
1
GR_RLA (GAPI) 0. 300.
HCAL (IN) 6. 16.
Temp (F) 0. 300.
GR (GAPI) 40. 100.
BS (IN) 6. 16.
Washout
Mudcake
2
TENS 406000.
DEPTH FT
11700
11750
3
RLA5 (OHMM) 0.2 2000.
RXOZ (OHMM) 0.2 2000.
LLS_G (ohm.m) 0.2 2000.
KINT_ELAN (MD) 0.02 200.
KA400shift () 0.02 200.
4
NPHI (V/V) 0.45 -0.15
RHOZ (G/C3) 1.9 2.9
DTCO (US/F) 140. 40.
PIGN_ELAN (V/V) 0.45 -0.15
PEFZ (B/E) 0. 20.
CPOR400shi () 45. -15.
5
Sw_Archie () 0. 1.
Swshifted (V/V) 0. 100.
6
T2_DIST_SH4 0 ( ) 64
T2CUTOFF 0.5 (ms) 3000
7
FMI_Imagen Dinami
Orientation North
0 120 240 360
Water
Oil
Calcite
Dolomite
Quartz
Bound Water
Clay
ELAN_VOLUMES ELAN_PVP_OU
1 (V/V) 0

Figure 3.12. Petrophysical Assessment in the key well (BOR-31). Track 1: Lithology, borehole quality, and temperature logs. Track 2: Depth and Tension measurements. Track 3: High-Resolution Laterolog Array measurements, RLA5, Shallow Laterolog Resistivity measurement, LLS, estimated from High-Resolution Laterolog Array Tool, RLA2 and RLA3, and modified Jennings' and Lucia's permeability (green line) and core permeability (red circles). Track 4: Neutron (dotted green line) and Density (blue line) logs, sonic log (fuchsia line), calculated effective porosity (red line) and core porosity (blue circles). Track 5: Archie's calculated water saturation (black line) and core water saturation (blue circles). Track 6: Nuclear magnetic resonance T_2 distribution and cutoff. Track 7: Image log, Formation Micro Imager (FMI) showing layers with variable thickness (1 to 5.5 ft), with massive appearance and development of vuggy porosity showing interconnection between poral spaces through fractures and microfractures observed from 11714 to 11717 ft. Track 8: Volumetric analysis showing the degree of heterogeneity of the carbonate reservoir. The computed mineralogy is consistent with that obtained from X-ray diffraction analysis.

CHAPTER 4

Numerical Simulation of the Process of Mud-Filtrate Invasion

This chapter presents the theoretical background for the process of mud-filtrate invasion. We also perform resistivity modeling to simulate the invasion process. Finally, we describe results from the simulation of mud-filtrate invasion in a key well, including its integration with rock-core measurements and special well logs.

4.1 THEORETICAL BACKGROUND

Quantitative assessment of the process of mud-filtrate invasion is an important step in the interpretation of resistivity logs across permeable layers (Dussan et al., 1994). Resistivity measurements are usually acquired at different radial lengths of investigation to characterize and estimate invasion. Mud-filtrate invasion is a process that occurs in permeable rock formations drilled by a well subject to overbalanced pressure caused by mud circulation (Wu et al., 2005). The length of invasion is the radial distance penetrated by the mud filtrate into the formation (Salazar et al., 2005). Radial length of invasion is influenced by mud (density, chemical composition and content of solids, circulation pressure, and time of filtration) and reservoir rock (porosity, permeability, relative permeability, pore pressure, rock fabric, capillary pressure, and residual fluid saturations) properties (Wu et al., 2005).

4.2 SIMULATION SOFTWARE FOR MUD-FILTRATE INVASION: UTFET

Numerical simulation of resistivity measurements in this thesis is performed with the University of Texas at Austin's Formation Evaluation Toolbox (UTFET). It is a 2D cylindrical simulator that considers two phases: oil and water (Ramirez et al., 2006; Salazar et al., 2007; Malik et al., 2007). The simulator is used for the estimation of flow rate of mud-filtrate invasion for given mud, rock, and fluid properties (Wu et al. 2005).

Initial properties of the reservoir in each well are obtained by applying the previously described multi-mineral approach. Subsequently, we apply the initial petrophysical values to the base case and proceed to numerically simulate resistivity measurements following the procedure described by Salazar et al. (2006), adapted in this study to mode dual-Laterolog (DLL) measurements. For the numerical simulation, we apply Brooks-Corey's capillary-pressure and relative-permeability curves (Corey, 1994) adjusted to the rock-core data showed in Figure 4.1. Depending on the presence of secondary porosity and/or permeability, the matching process may require successive perturbations to porosity and permeability. Figure 4.2 shows a diagram of the procedure implemented with the FET to perform numerical modeling of the process of mud-filtrate invasion.

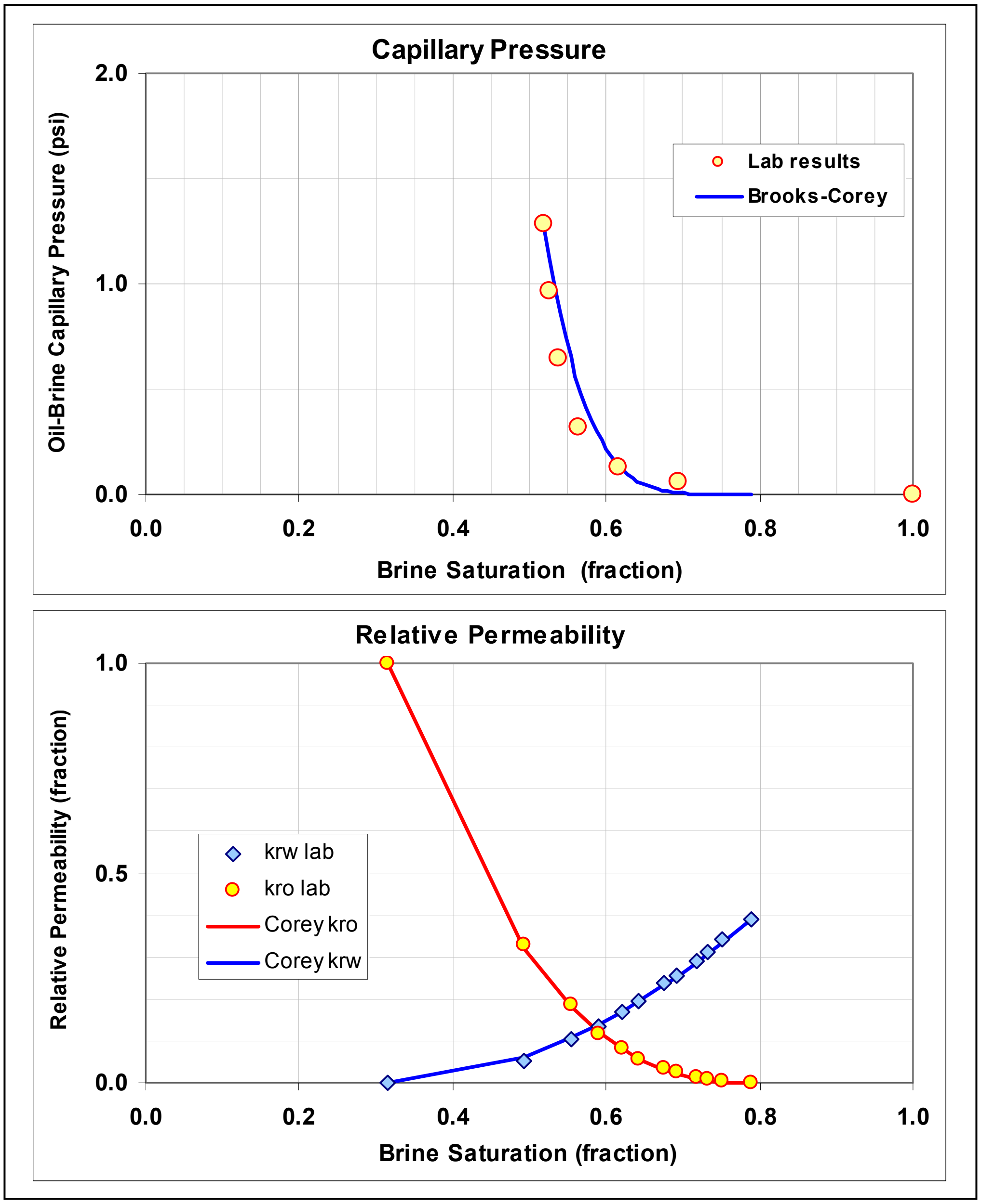

Figure 4.1. Match of Brooks-Corey's oil-brine capillary pressure and relative permeability curves with laboratory core measurements.

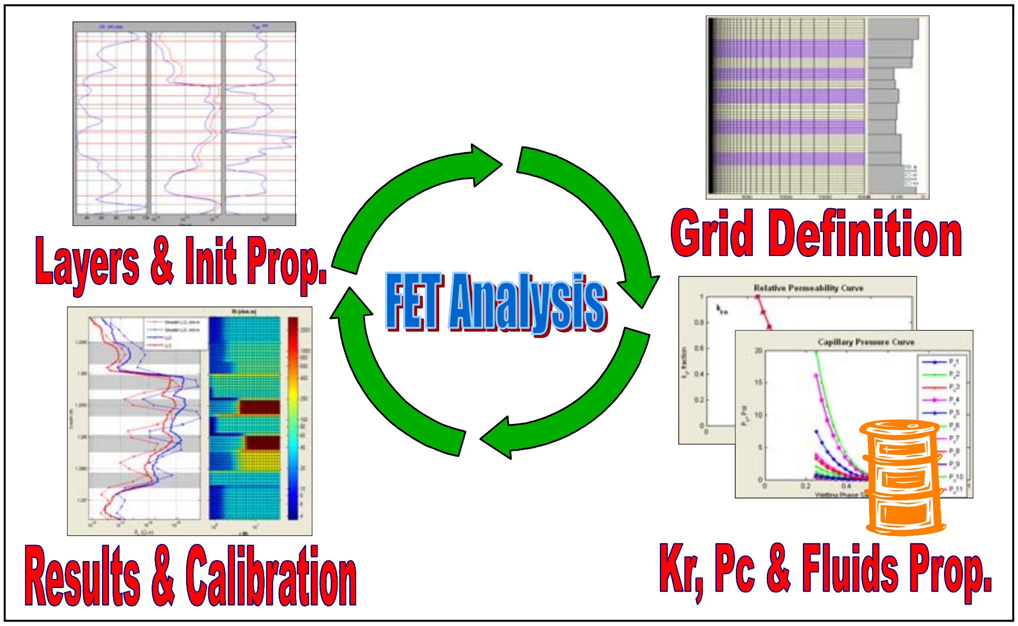

Figure 4.2. Diagram of the procedure followed by the FET to model the process of mud-filtrate invasion.

4.3 RESISTIVITY MODELING PERFORMED PRIOR TO MUD-FILTRATE INVASION MODELING

We previously described in Chapter 2 the wide variety of resistivity logs acquired in "O BOR 2E" reservoir with both WBM and OBM. Our results depend on matching simulated apparent resistivity curves with field measurements. Therefore, we perform resistivity modeling before mud-filtrate invasion modeling in order to determine which resistivity tools are more appropriate for this study. Resistivity modeling and inversion are usually performed to estimate invaded-zone and undisturbed-zone resistivity, and radial depth of invasion (Salazar et al., 2007). Resistivity modeling is performed using the University of Texas at Austin's Borehole Resistivity Modeling Toolbox (BRT). The

BRT simulates and inverts borehole laterolog, induction, and spontaneous potential (SP) measurements for the case of multiple horizontal layers penetrated by a vertical well. It also includes several radial zones with different values of electrical conductivity for each horizontal layer. Such piston-like radial variations of electrical conductivity enable the simulation of the effect of mud-filtrate invasion (Wang and Torres-Verdín, 2006). We follow the procedure applied by Wang and Torres-Verdín (2006) to study the various cases considered in this thesis.

First, we perform resistivity modeling on a synthetic case with homogeneous properties and without invasion for two types of tools: Dual-Laterolog (DLL) and Array-Induction Tool (AIT). Figure 4.3 shows results obtained for both cases (Panels c and d show results for DLL and AIT, respectively). Then, we perform the same processing in one of the available wells with DLL measurements, and considering a homogeneous interval with no invasion. Figure 4.4 displays the results obtained for this case, indicating a good match between modeled apparent resistivities and field measurements.

As expected, the separation of resistivity curves is negligible for this case because we assume no invasion. We observe such a behavior when we model the DLT resistivities (Figure 4.3.c). However, when simulations are performed with the AIT, the simulated curves exhibit a significant separation (Figure 4.3.d). The same observation applies to other cases considered in Borburata field but not shown in the study. In addition, “O BOR 2E” is a carbonate reservoir with a low-porosity matrix that causes high-value readings of resistivity measurements. Moreover, in the presence of OBM, resistivity readings can be even higher with values well above 1000 Ohm-m. Such conditions are other limitations for induction tools. Based on results obtained, we only apply our method in wells with resistivity logs acquired with WBM such as DLL and High-Resolution Laterolog Array Tool (HRLT).

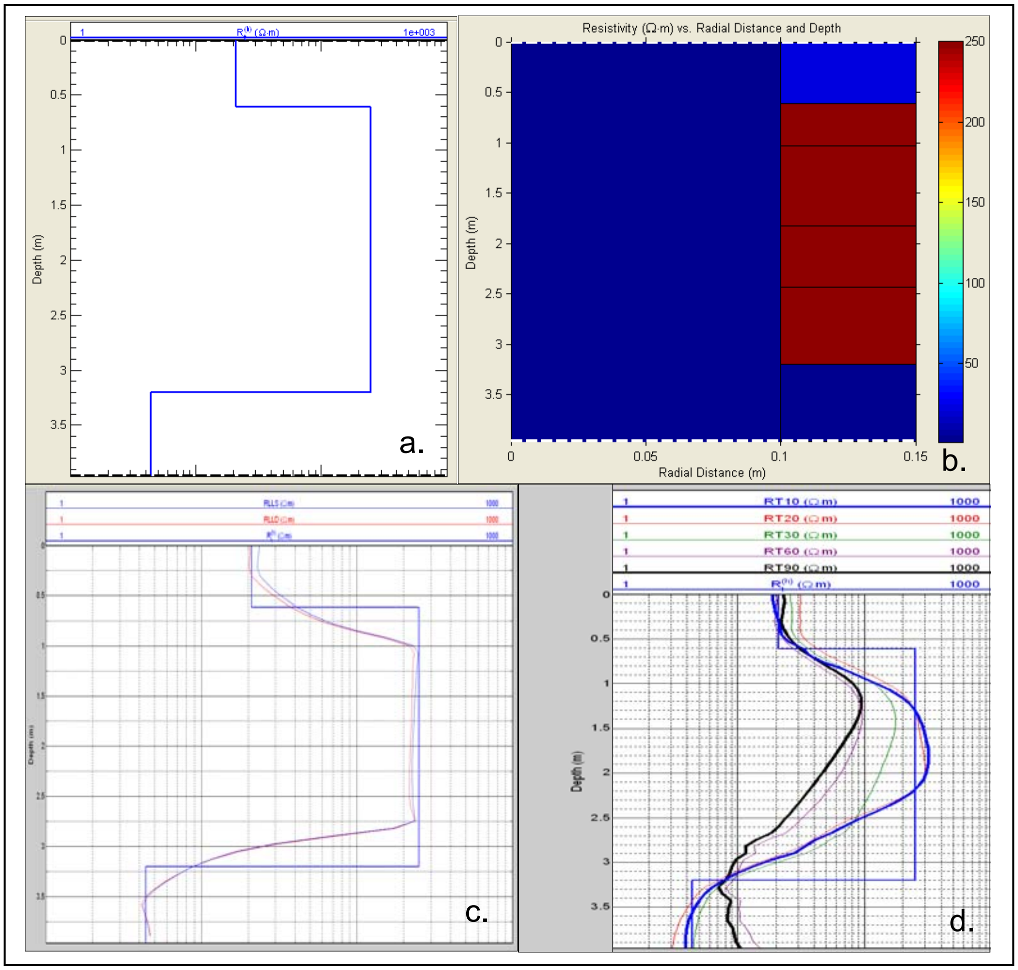

Figure 4.3. Resistivity modeling results before numerical modeling of the process of mud-filtrate. The figure shows resistivity modeling results considering a synthetic case with homogeneous properties. Panels a and b show a synthetic earth model without invasion. Panels c and d show results obtained for DLL and AIT, respectively.

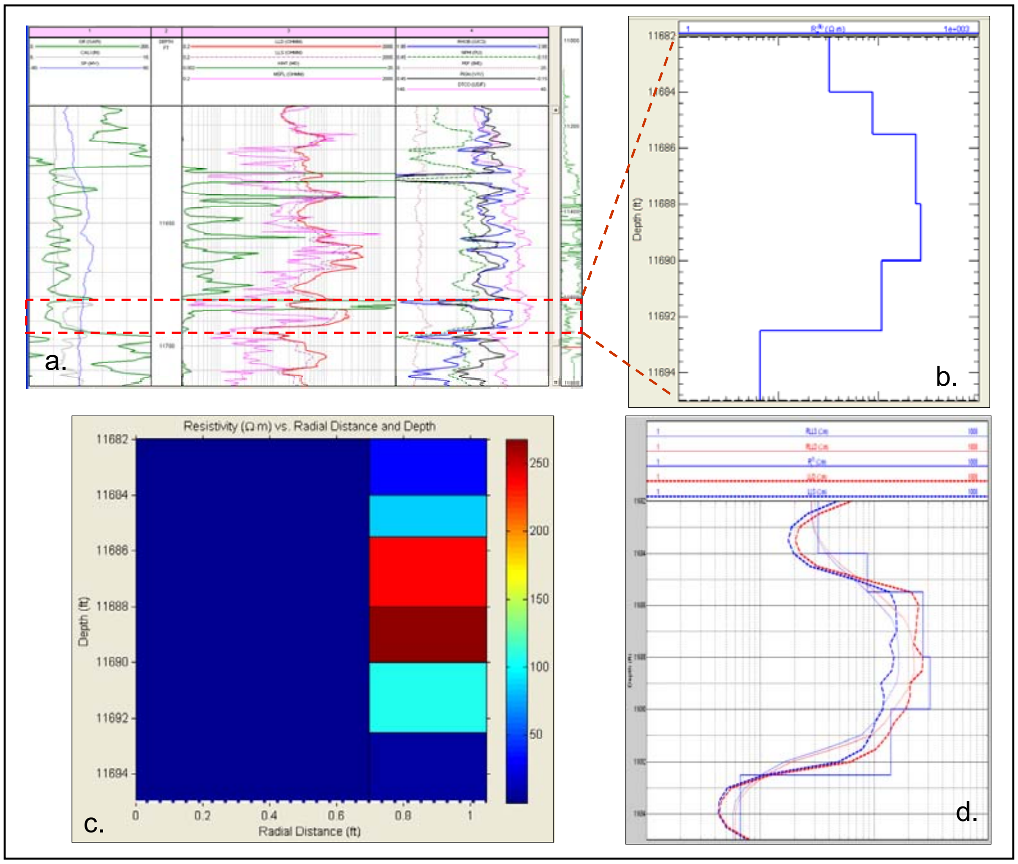

Figure 4.4. Resistivity modeling results before numerical modeling of the process of mud-filtrate. The figure shows resistivity modeling results considering a field case with homogeneous properties. Panel a shows the depth interval selected for the construction of the earth model. Panels b and c show the earth model without presence of invasion. Panel d shows results obtained from DLL resistivity modeling.

4.4. SIMULATION OF MUD-FILTRATE INVASION IN THE KEY WELL

We start with a description of a simple case where we apply our method. This case enables us to understand the basics behind the simulation of mud-filtrate invasion to diagnose fractured and vuggy carbonate formations. We consider a well (BOR-12) that was logged with a DLL tool and drilled with WBM with salinity of 33000 ppm approximately. Core data were available for this case of study. Initial properties of the reservoir in well BOR-12 were obtained by applying a multimineral approach. Subsequently, we applied initial petrophysical values to the base case and proceeded to numerically simulate resistivity measurements following the procedure explained by Salazar et al. (2006) and adapted to DLL measurements. For the numerical simulation, we applied Brooks-Corey's model adjusted to rock-core data for capillary pressure and relative permeability.

Figure 4.5 is a geometrical description of the finite-difference grid implemented for the simulation of the process of mud-filtrate invasion and resistivity measurements. The figure also includes the flow units considered. We only used 3 different layers because we have a simple case. Each layer has its own rock property values such as effective porosity, absolute permeability, and irreducible water saturation among others. The simulation grid implemented here consisted of 30 x 31 nodes in the radial (r) and vertical (z) directions, respectively. We consider the previous type of grid with several numerical layers to account for property changes and improve simulation results. In addition, our grid consists of logarithmically distributed nodes to consider appropriate spatial resolution for the evolution of mud-filtrate invasion near the wellbore as a function of time. Appendix B describes the meaning of parameters considered in the

Brooks-Corey equations. It also contains a summary of the parameters used in the BOR-12 case for modeling capillary pressure and relative permeability.

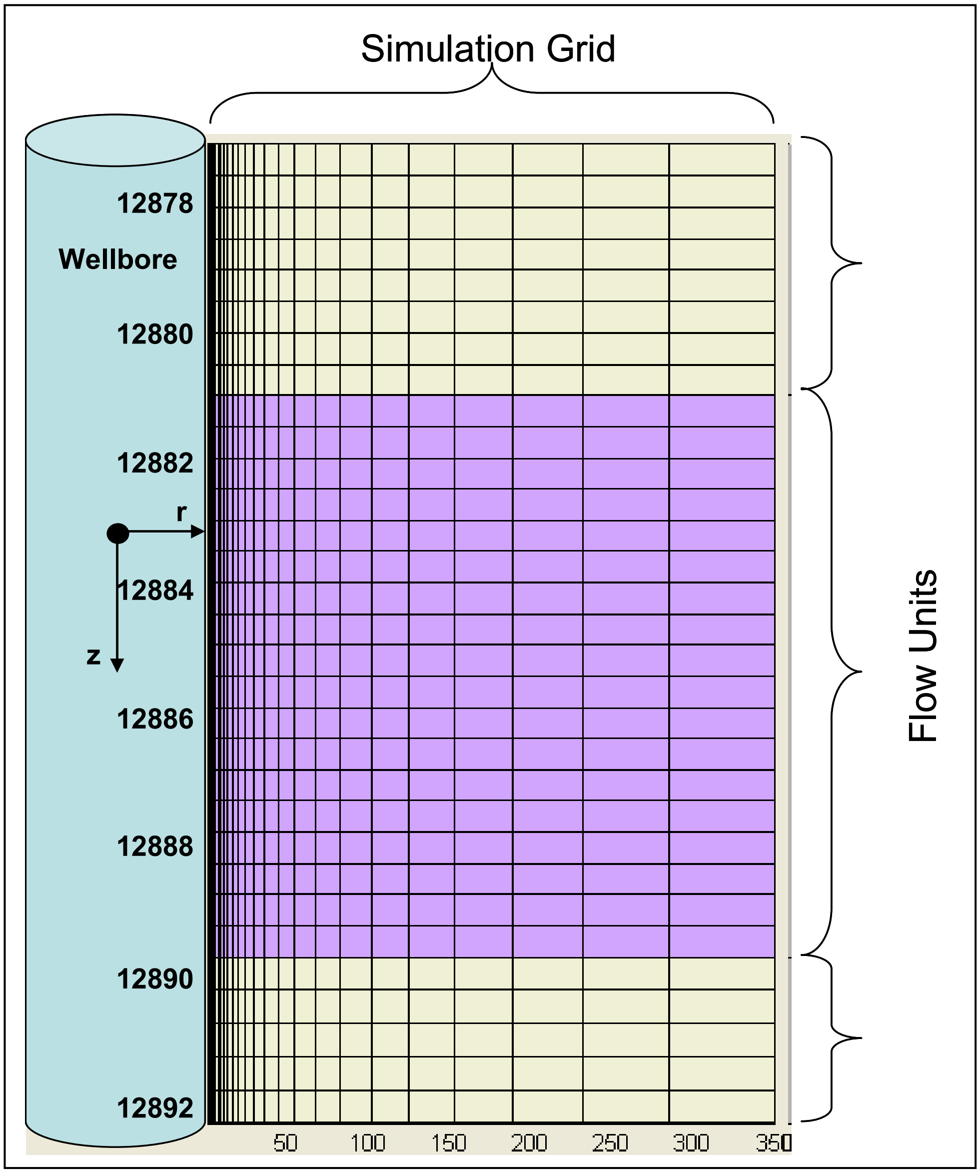

Figure 4.5. Geometrical description of the finite-difference grid implemented for the simulation of the process of mud-filtrate invasion. This figure also includes the flow units considered in the modeling.

4.5 SIMULATION RESULTS

Figure 4.6 shows simulation results considering permeability obtained from rock-core measurements (left-hand side panel) and those for the case of permeability obtained from pressure transient measurements (right-hand side panel). The best match required an increase of both permeability and porosity as shown in Figure 4.6. The increase of porosity is explained by the fact that, according to the interpretation of core data, a massive dolomitization took place in the simulated interval. Sin-sedimentary and diagenetic fractures are also observed as well a high density of vugs with a large variety of sizes (micro to megavugs).

The main porosity on the simulated interval is due to the system of vugs which also connect the rest of the porosity provided by the matrix and fractures. Figure 4.7 shows some details of these features with a photograph of core taken in well BOR-12. We highlight the presence of vugs and fractures in figure 4.7. In addition, a high dolomitization process derived from an arid tidal flat (sabkha) environment took place in the interval (Figure 3.1). This is one of the main flow units in the well and facies contained here have intercrystalline, intracrystalline, moldic and vuggy porosity as shown in the thin sections of Figure 3.2. The diameter of the vugs varies from millimeters to centimeters. Most of the oil is stored in the previously described types of porosity. The oil deposited there is being produced by communication provided by the intercrystalline and intracrystalline porosity and fractures, according to previous sedimentological studies (Mendez, 2002; Kupecz et al., 2000).

According to a previous study performed in the same core (Corpro, 2000); the permeability in the fractures has a wide range, between 500 to 12000 mD. One of the most important conclusions from the Corpro study is that many of the fractures are related to vuggy zones. The amount of permeability provided by these fractures and interconnected vugs and the effect on total permeability is explained by Aguilera (1995) and Lucia (2007).

The improvement in permeability and porosity is due to the fact that fractures and vugs are important components of the storage and flow capacity of reservoirs with double or triple-porosity systems such as the one under study. Similar results are emphasized by Aguilera (1995) considering that a reservoir with a matrix permeability equal to 1mD may entail an average permeability for the system equal to 14 mD taking into account presence of vugs with a diameter of 0.05 in. Aguilera also describes a reservoir with a matrix permeability equal to 1 mD that could have an average permeability of the system equal to 13.51 Darcies considering presence of 3 fractures, each one 0.01-in wide. Therefore, quantifying porosity and permeability due to such artifacts would provide a more reliable and accurate description of petrophysical properties in carbonate reservoirs.

The permeability obtained through our method of simulation of mud-filtrate invasion **(101.36 mD)** agrees with the permeability estimated from pressure transient measurements **(101 mD)**, which is believed to be the best representation of permeability of the system (matrix + vugs + fractures). Details and results obtained from this test are covered in section 2.5 of Chapter 2.

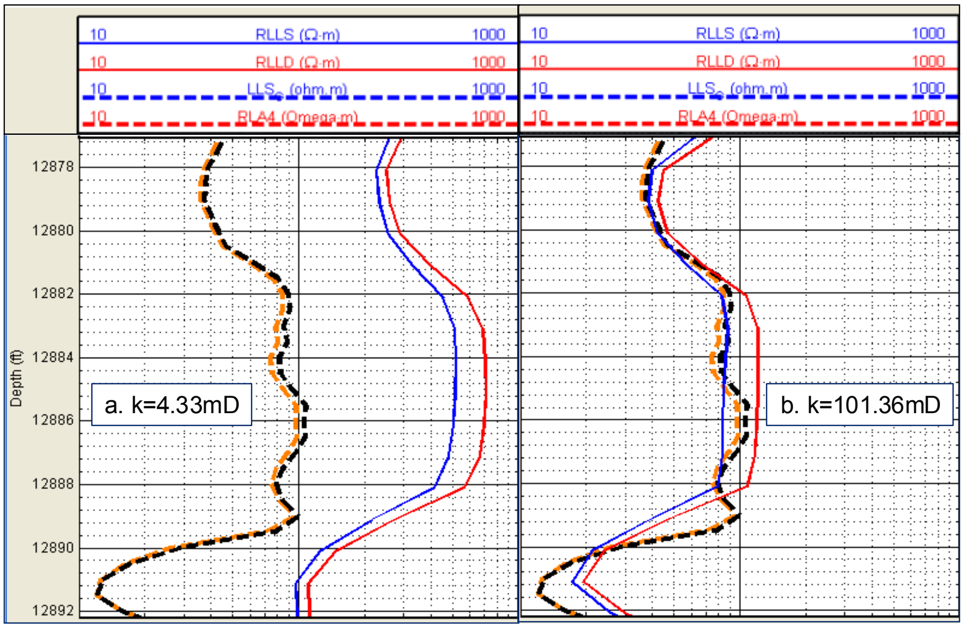

Figure 4.6. Numerical simulation of DLL measurements for well BOR-12. The left-hand side panel shows field (dashed) and simulated (continuous) resistivity curves for the case of permeability obtained from rock-core measurements. The right-hand side panel shows field (dashed) and simulated (continuous) resistivity curves for the case of permeability obtained from pressure transient measurements. For the second case, we considered a perturbation of porosity.

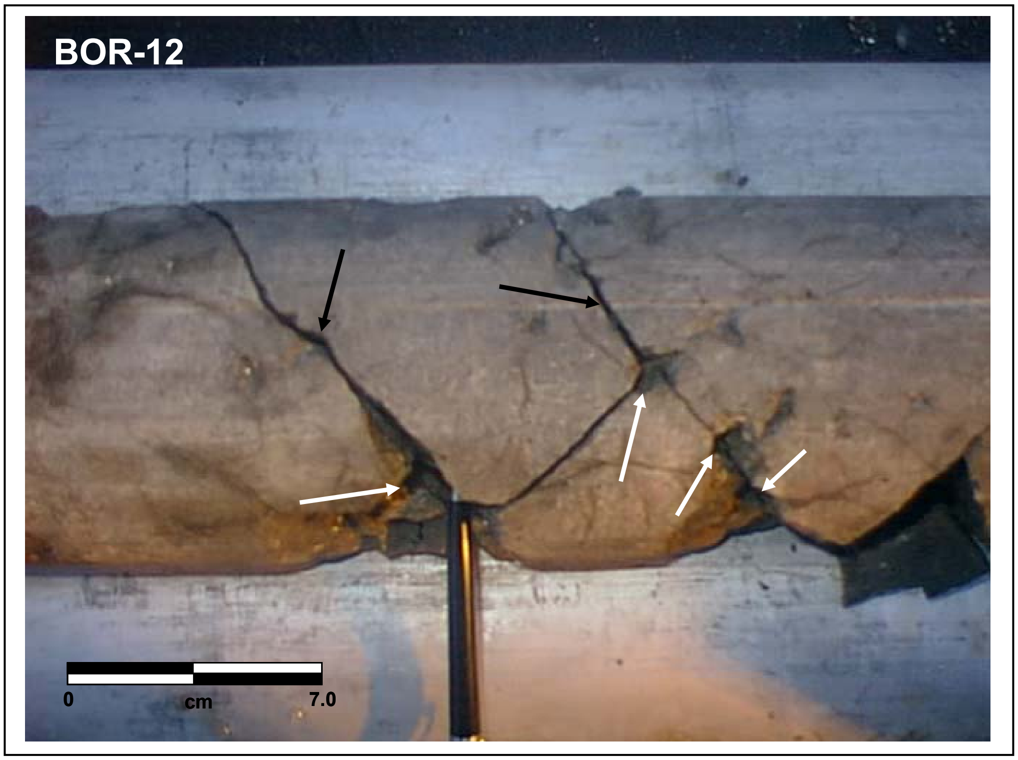

Figure 4.7. Core photograph taken in well BOR-12. The sample covers part of the depth interval considered in the numerical simulations of mud-filtrate invasion. White arrows indicate presence of vugs while black arrows indicate fractures.

Finally, we propose a model developed for the estimation of secondary porosity and permeability. Figure 4.8 shows a cross-plot of permeability (k, mD) versus porosity (Φ, %), including parametric curves of constant k/Φ ratios that we used to explain the results for this particular case. The plot considers rock-core measurements corresponding to well BOR-12.

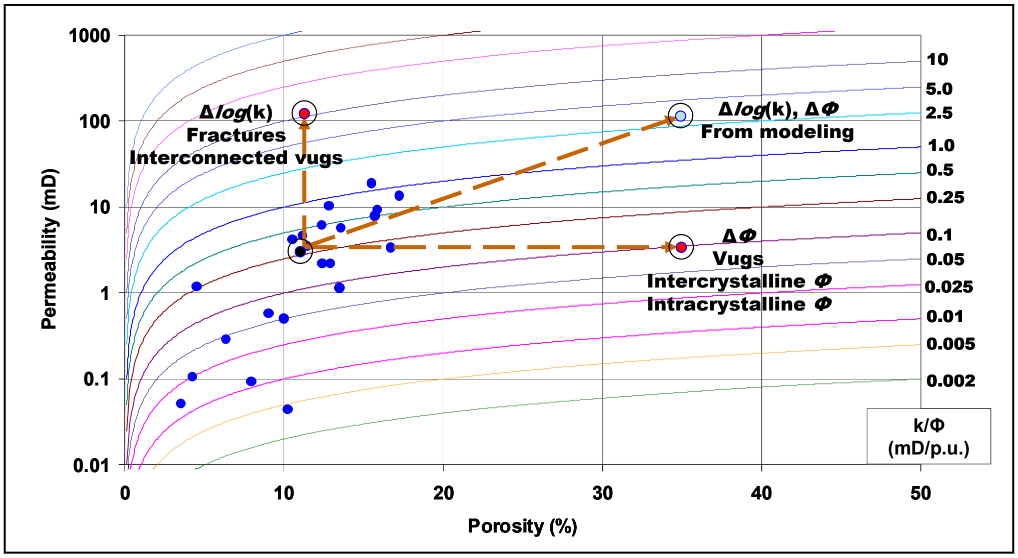

Figure 4.8. Theoretical model developed for the estimation of secondary porosity and permeability. Blue circles represent porosity and permeability obtained from rock-core data (plugs). Black circles identify initial average rock properties obtained from rock-core measurements. Red circles indicate perturbations of initial permeability and porosity due to presence of fractures, interconnected vugs, intercrystalline and intracrystalline porosity, or combination of any of these features. The light blue circle identifies permeability and porosity values obtained from mud-filtrate invasion modeling.

In this plot we show the average rock properties obtained from rock-core measurements (black circle) used to initiate the simulation. We also show how the presence of fractures, interconnected vugs, intercrystalline and intracrystalline porosity, or a combination of any of these features can cause perturbations of initial values permeability and porosity (red circles). We also include permeability and porosity values obtained from mud-filtrate invasion modeling for the simulated depth interval (light blue circle).

The previous remarks indicate that simulation of mud-filtrate invasion can be applied to diagnose and estimate secondary porosity and permeability due to vugs and fractures via the model shown in Figure 4.8. Presence of non-connected vugs would be associated with those cases where major changes of porosity are needed to fit the field data via forward modeling. Presence of connected vugs and fractures would be estimated for those cases where significant modifications of permeability from the base case would be needed to match the measurements. There could also be a combination of both cases (Figure 4.8), as it was shown in the previous case.

CHAPTER 5

Mud-Filtrate Invasion Modeling To Diagnose and Quantify Fractured and Vuggy Carbonate Formations

This chapter describes the application of the method introduced in Chapter 4 to two additional wells. Results from Chapter 4 are extrapolated to a well that includes advanced well logs but no rock-core measurements. In addition, a third case is included from a well considered key to the study because of the amount and quality of information available (rock-core measurements and advanced well logs). The case enables us to integrate all the available data to improve the interpretation. Finally, we show results obtained from the simulation of mud-filtrate invasion and compare them to permeability values obtained from other methods or measurements.

5.1 MUD-FILTRATE INVASION MODELING IN WELL 2

We consider a well (BOR-11) close to the key well studied in Chapter 4. The well is located at a distance of 400 m from well BOR-12 (Figure 2.11). Well BOR-11 was also logged with a DLL tool and drilled with WBM with the same salinity of the previous case. Core data were not available for this case; however, advanced well logs were acquired in well BOR-11 (image and sonic logs). We perform a petrophysical assessment based on the previously described method for key well BOR-12. Subsequently, we applied initial values for rock properties and then proceeded to numerically simulate resistivity measurements following the same procedure presented in Chapter 4. Petrophysical parameters and data such as capillary pressure and relative permeability from rock-core measurements are obtained from the previous case. For the numerical simulation of well BOR-11 we consider 4 flow units that are divided into a number of layers (7) to represent property changes and improve simulation results. The simulation grid implemented has the same characteristics of previous case (Well 1, Chapter 4).

5.2 DIAGNOSIS AND QUANTIFICATION OF FRACTURED AND VUGGY CARBONATE FORMATIONS IN WELL 2

Our method to estimate secondary porosity and permeability in fractured and vuggy carbonate formations is based on the numerical simulation of the physics of mud-filtrate invasion and consists of performing the simulation with initial rock properties (porosity and permeability) estimated from well-logs correlations. Then, progressive perturbations on these properties are made until we secure a match between simulated and measured apparent resistivities. Figure 5.1 shows simulation results obtained by considering permeability estimated from well-logs correlations (left-hand side panel) and those for the case of permeability estimated through simulation of the mud-filtrate invasion process (right-hand side panel). Figure 5.1 shows the increase in permeability needed to secure the best match between simulated and field measurements resistivities. Figure 5.1 also shows that for this case, the initial estimation of porosity is sufficient to achieve an accurate agreement between simulated and measured apparent resistivities.

Figure 5.2 displays an image log (FMI) acquired in well BOR-11 showing simulated interval. The increase of permeability is explained by the interpretation of image logs where we observe the presence of vugs and fractures that might be connecting the vugs, therefore, causing an increase in permeability for the system. According to previous studies (Mendez, 2002; Kupecz et al., 2000), wells BOR-12 and 11 would be in a similar quality zone. Mendez (2002) and Kupecz et al. (2000) studies indicate the presence of sin-sedimentary and diagenetic fractures for the same area with a high density of vugs with different sizes (micro to megavugs) that would contribute to increase the reservoir quality.

Figure 5.3 shows a distribution of reservoir quality of cycles 1' and 1 in the Borburata field. Our simulation in wells BOR-11 and 12 was performed in intervals corresponding to the same cycles. In the plot of Figure 5.3, the red area represents zones with higher porosity and permeability and presence of principal flow units with high reservoir quality. The pink zone indicates zones where lower porosity was observed in cores. In addition, Mendez (2002) detected reservoirs with low quality and secondary flow units in these zones. The previous conclusion is based on core observations, well-logs interpretation and production data (Mendez, 2002).

Therefore, permeability contribution from fractures observed in core from well BOR-12 (Corpro, 2000) can be extrapolated to the case of well BOR-11 that is located within a close distance and it is with a zone with similar sedimentological characteristics.

Average permeability obtained through simulation of mud-filtrate invasion **(134.26 mD)** is significantly higher than average permeability estimated from well-logs correlation **(6.12 mD)** for the interval analyzed. Considering that wells BOR-11 and 12 are located in zones with related geological characteristics, with presence of vugs and fractures interconnecting them, we believe that permeability obtained from our simulations is the best representation of permeability for the system (matrix + vugs + fractures). It is also important to emphasize that well BOR-11 is the best producer in

Borburata field (See Chapter 2, section 2.6). It started producing up to 4000 bpd and has a current production close to 2000 bpd after more than 9 years of production. Production of well BOR-11 confirms the high reservoir quality of this zone provided by the presence of fractures and interconnected vugs.

Figure 5.4 shows results for the case of well BOR-11 in our theoretical model previously explained. Once again, the model confirms that perturbations on initial petrophysical properties are needed to secure a good match between resistivity from simulations and field measurements. For the present case, we only needed to perform perturbations of permeability.

Results obtained in the case of well BOR-11 confirm that simulation of mud-filtrate invasion can be applied to estimate permeability for reservoirs where fractures and interconnected vugs improve reservoir quality. Previous results would indicate the presence of connected vugs and fractures because significant modifications of permeability were needed for the base case to match the available apparent resistivity curves.

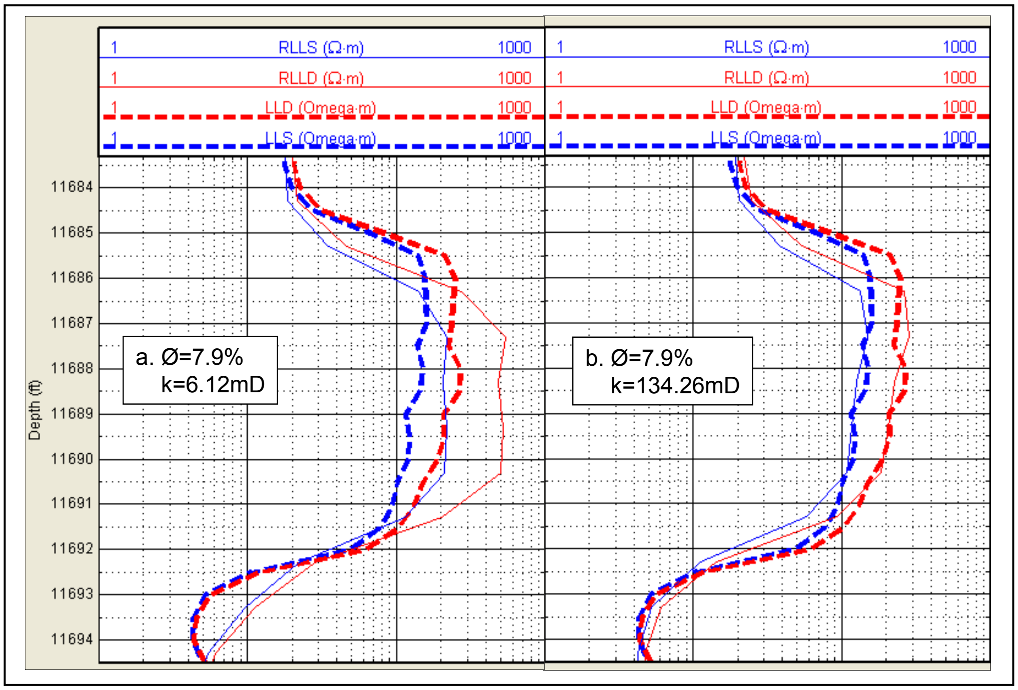

Figure 5.1. Numerical simulation of DLL measurements for well BOR-11. The left-hand side panel shows field (dashed) and simulated (continuous) apparent resistivity curves for the case of permeability estimated from well-log correlations. The right-hand side panel shows field (dashed) and simulated (continuous) apparent resistivity curves for the case of permeability estimated from the simulation of mud-filtrate invasion.

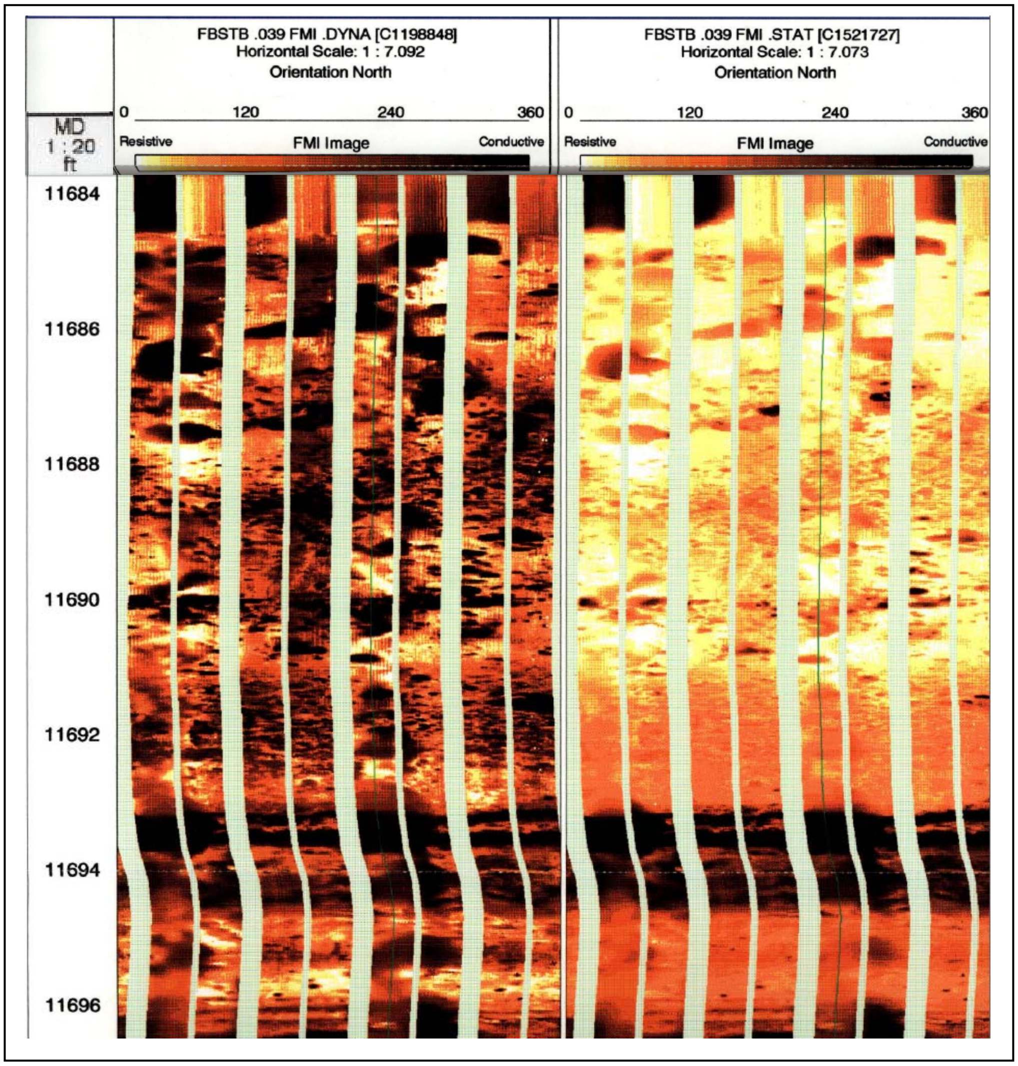

Figure 5.2. Image log (FMI) acquired in well BOR-11. Left-hand side panel shows dynamic images obtained from the simulated depth interval. The right-hand side panel shows static images acquired from the same interval.

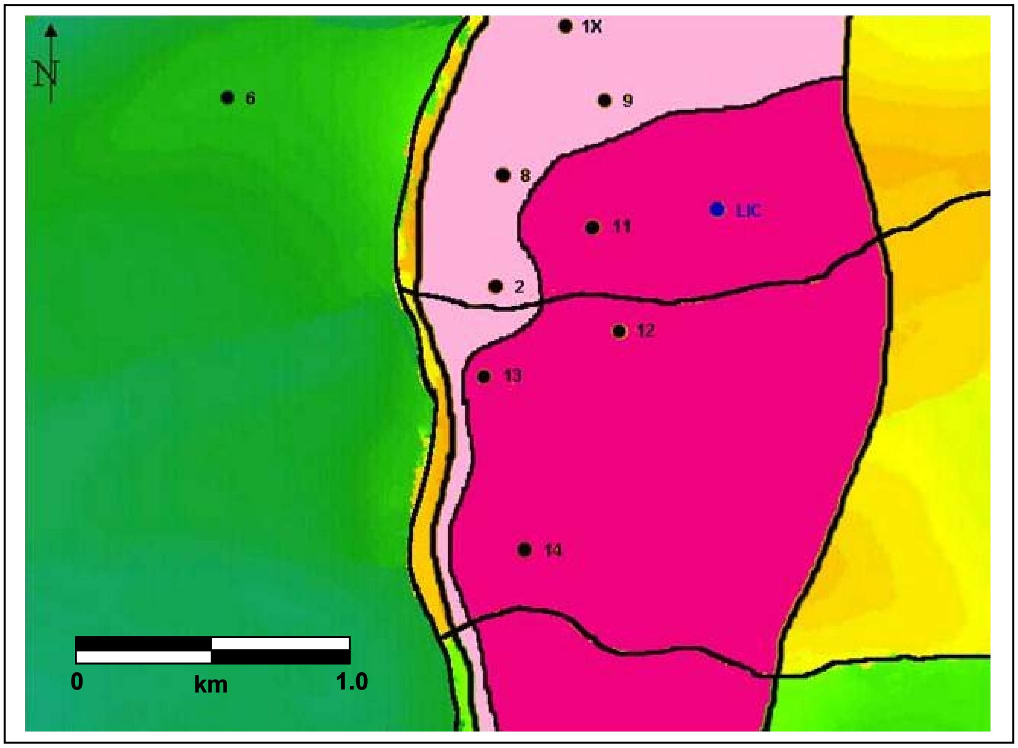

Figure 5.3. Distribution of reservoir quality for cycles 1' and 1 in Borburata field. The red area indicates zones with high porosity and permeability values and presence of principal flow units with high reservoir quality. The pink area shows zones where low porosity values were observed in cores. In addition, reservoirs with low quality and secondary flow units were detected in the pink area from core observations, well-log interpretation and production data (modified from Mendez, 2002).

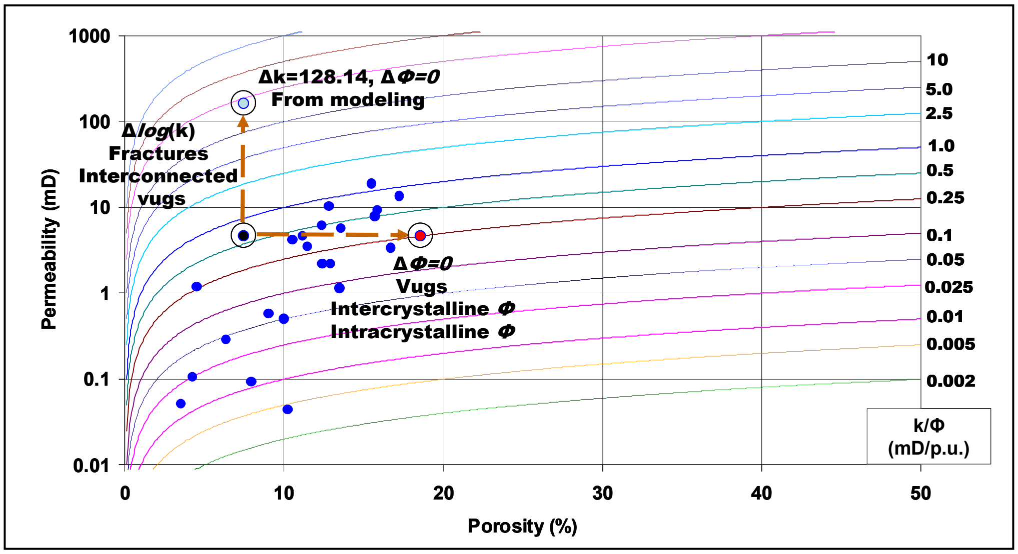

Figure 5.4. Application of the simulated model to the estimation of secondary porosity and permeability in well BOR-11. Blue circles represent porosity and permeability obtained from rock-core data (plugs) in well BOR-12. Black circles indicate the initial average rock properties estimated from well-log correlations. Red circles represent required perturbations on initial permeability and porosity due to presence of fractures, interconnected vugs, intercrystalline and intracrystalline porosity, or the combination of any of these features. The light blue circle indicates permeability and porosity obtained from mud-filtrate invasion modeling.

5.3 MUD-FILTRATE INVASION MODELING IN WELL 3

We apply the method on other case following the same steps previously described in Well 1. We consider a well (BOR-31) that is apart from the remaining two wells described earlier. This well is located at a distance of 3.6 km from well BOR-12 (Figure 2.11). However, well BOR-31 is considered key in our study because of the amount and quality of information available (rock-core measurements and advanced well logs). The case of Well 3 enables us to perform an appropriate integration of available data to obtain reliable results and a more precise understanding of the process of mud-filtrate invasion in vuggy and fractured reservoirs. The simulation is performed in a similar manner to previous cases.

Well BOR-31 was logged with a High-Resolution Laterolog Array Tool (HRLA) and drilled with WBM with the same salinity as in previous cases. Core data available for the present case enabled us to apply the same method of well BOR-12. Moreover, advanced well logs acquired in well BOR-31 (image, dipole sonic, 3-arm caliper, and nuclear magnetic resonance logs) provided a better understanding of necessary perturbations of permeability to obtain improved results.

We already described the petrophysical assessment for well BOR-31 in Chapter 3 based on our multi-mineral approach. Subsequently, we applied initial values for rock properties and proceeded to numerically simulate resistivity measurements following the same procedure already presented in Chapter 4. Some of the petrophysical parameters are obtained from the first case while data such as capillary pressure and relative permeability from rock-core measurements are available for the present case. We consider 5 flow units that are divided into 12 layers for simulation of well BOR-31.

5.4 DIAGNOSIS AND QUANTIFICATION OF FRACTURED AND VUGGY CARBONATE FORMATION IN WELL 3

For the case of Well 3, we did not have a code available to perform the forward modeling of the type of resistivity tool used in well BOR-31. However, we run our simulation considering a DLL tool. We compare HRLA and DLL available from the literature (Schlumberger, 2000). Figure 5.5 compares HRLA and HALS (High-Resolution Azimuthal Laterolog) resistivity field data vs. depth of mud-filtrate invasion.

The borehole-corrected HALS deep resistivity (HLLD) adequately compares with the Mode-5 response from the HRLA array measurement, while the HALS shallow resistivity (HLLS) is intermediate between the Mode-2 and Mode-3 HRLA responses. The additional HRLA resistivity measurements allow us to identify resistivity changes resulting from mud-filtrate invasion. As a result, we consider the RLA5 field measurement as HLLD while the HLLS response was estimated from a geometric average of RLA2 and RLA3 responses.

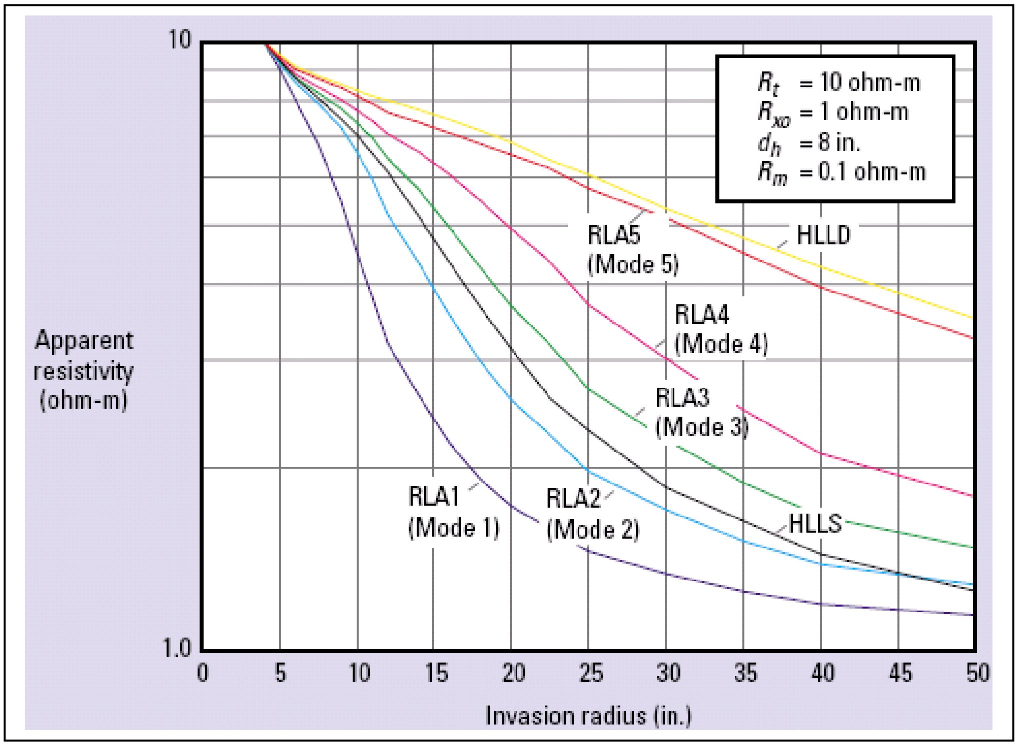

Figure 5.5. HRLA (High-Resolution Laterolog Array Tool) and HALS (High-Resolution Azimuthal Laterolog) resistivities vs. radial length of mud-filtrate invasion. Comparison of HRLA and DLL resistivity field data (Schlumberger, 2000). RLA5 from the HRLA tool is comparable to HLLD from the HALS tool.

Figure 5.6 shows simulation results obtained for the case of well BOR-31. In this plot we consider permeability obtained from rock-core measurements to perform the simulation. Results are presented in the left-hand side panel. We consider successive perturbations of permeability and porosity to secure a match between simulated and field measurements resistivities. Results for the later case are presented in the right-hand side panel in Figure 5.6. In the same figure we show that the best match required a significant increase of permeability from initial properties. We consider small perturbations of porosity in some layers of this well. The increase of permeability is explained from the interpretation of core data and image logs acquired in well BOR-31. Through interpretation of image log we observe dolomitized facies in the simulated depth interval with presence of vugs and partially conductive fractures. The vugs and fractures might be connecting the matrix and providing an increased permeability for the entire system. An observation of core data confirms the interpretation of image logs.

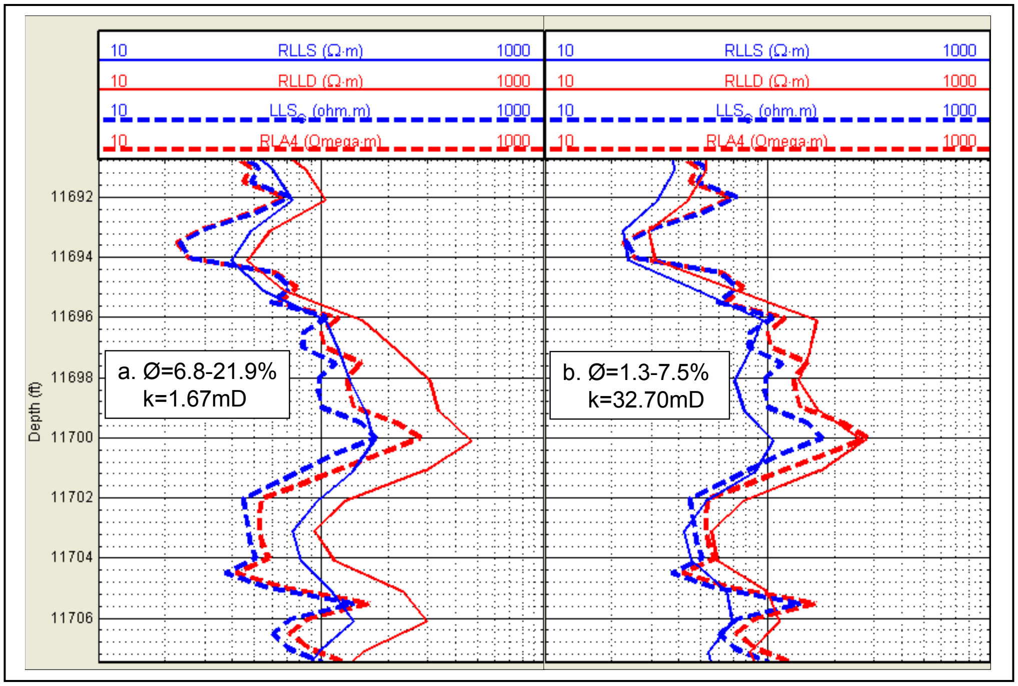

Figure 5.6. Numerical simulation of HRLA as DLL measurements for well BOR-31. The left-hand side panel shows field (dashed) and simulated (continuous) apparent resistivity curves for the case of permeability obtained from rock-core measurements. The right-hand side panel shows field (dashed) and simulated (continuous) apparent resistivity curves for the case of permeability obtained from pressure transient measurements. We consider perturbations of porosity in some layers of this well.

Figure 5.7 presents the image log (FMI) acquired in well BOR-31 showing the same depth interval where we simulated the mud-filtrate invasion process. We observe presence of dolomitized facies through interpretation of image log. It also shows presence of vugs (blue arrows) and partially-conductive fractures (red arrows). Figure 5.8 shows a zoom of the previous figure displaying more details where we highlight the presence of vugs (blue arrows) and fractures (red arrows).

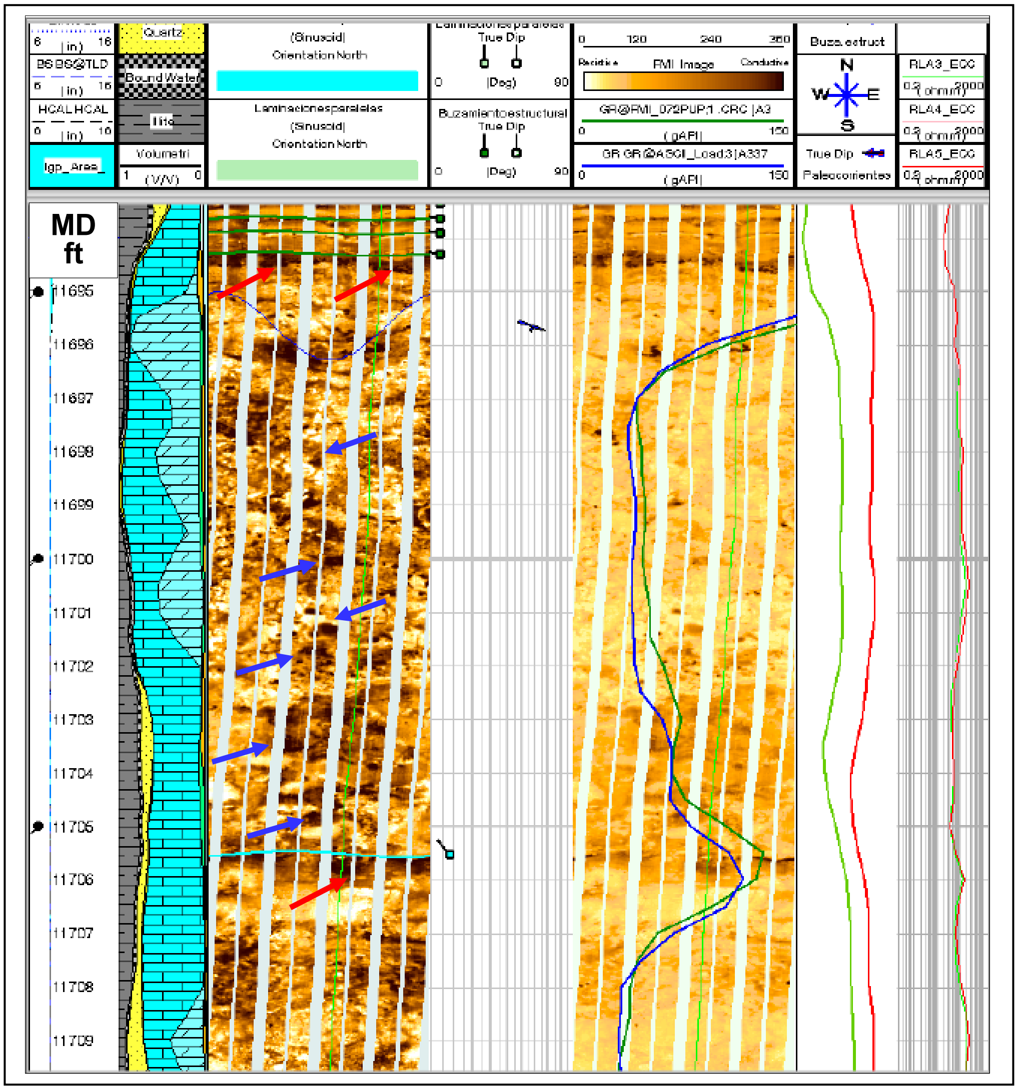

Figure 5.7. Image log (FMI) acquired in well BOR-31 showing the simulated depth interval. The picture shows presence of vugs (blue arrows) and partially-conductive fractures (red arrows).

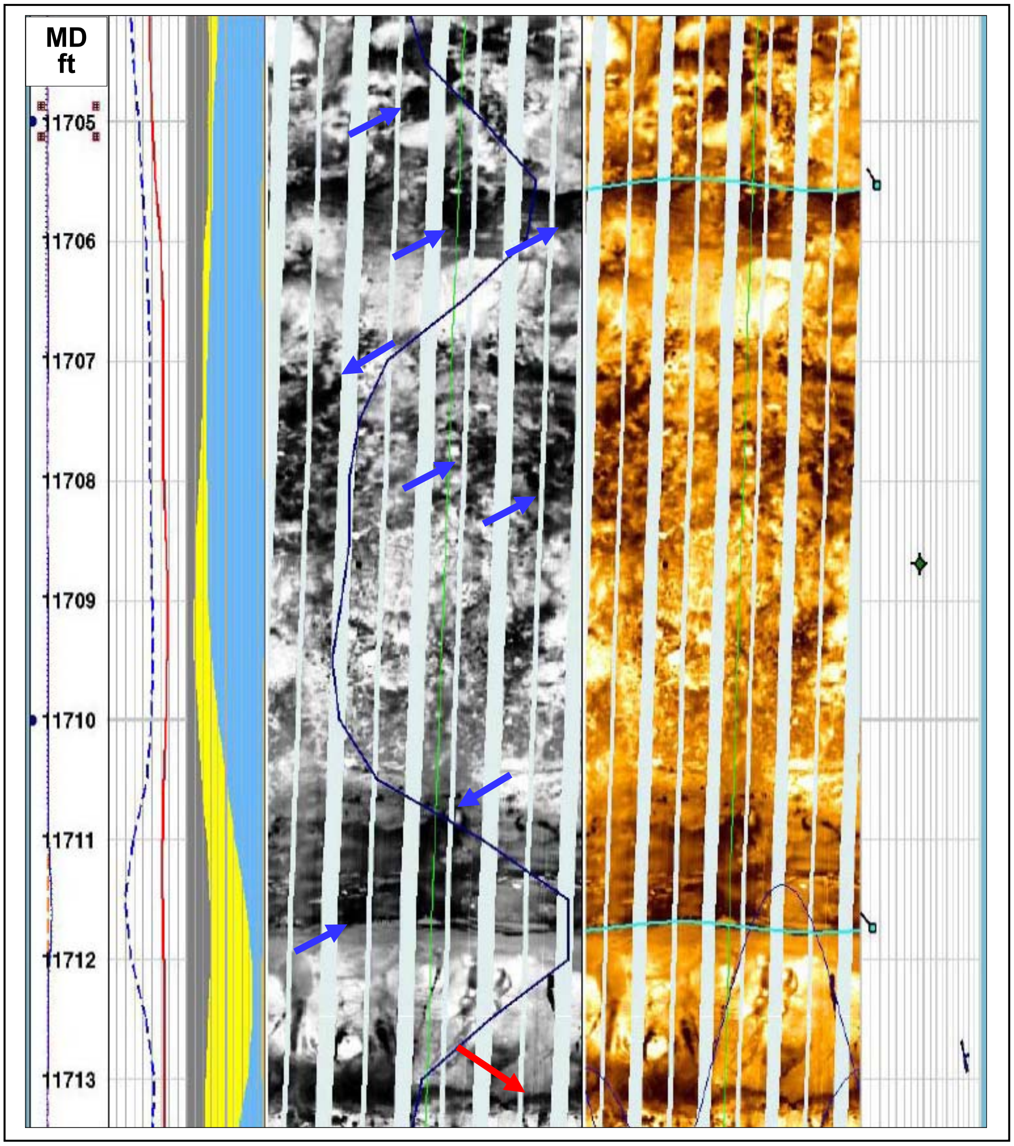

Figure 5.8. Image log (FMI) acquired in well BOR-31 showing more details of the same depth interval. The section displays the same features previously observed where we highlight presence of vugs (blue arrows) and fractures (red arrows).

Figure 5.9 shows pictures of core taken at the same depth. It is important to highlight that a depth difference exists between log and rock-core measurements. Observation of core data confirms the presence of a dolomitization process with vugs (blue arrows) and fractures (red arrows). While some vugs appear to be isolated, integration of core data and image logs indicate that others are interconnected. The integration also suggests the presence of secondary porosity and permeability for the simulated interval that would improve the total permeability and porosity of the system.

Average permeability obtained for the analyzed depth interval through simulation of mud-filtrate invasion **(32.70 mD)** is significantly higher than the average permeability from rock-core measurements **(1.67 mD).** We have already explained the main reasons for such changes. Previous results have a better representation of permeability of the system (matrix + vugs + fractures) according to observations of core data and integration with image logs.

For this interval we had to increase average permeability to secure a match between simulated and field resistivities. However, there were layers where we also had to make perturbations of porosity, thereby decreasing the values obtained from rock-core measurements. Porosity obtained from our simulation provides a better match with porosity obtained from well logs that ranges from 4 to 7%. Even though this zone is characterized for the presence of only one rock-fabric class (large crystal dolostones with average size of 300 μm approximately), presence of silt-sized quartz grains and clay minerals tends to reduce the effective porosity (Chapter 3, Figure 3.11).

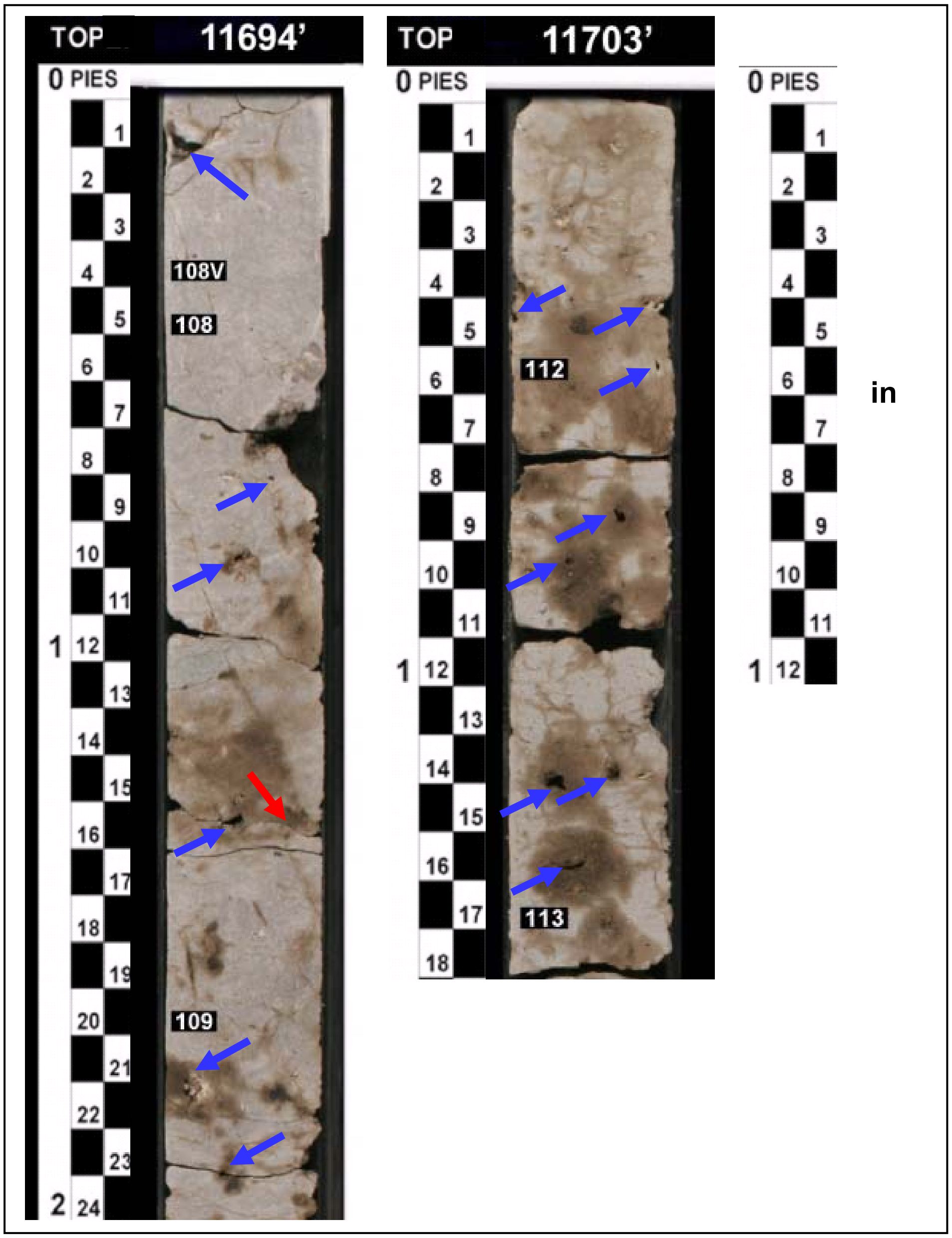

Figure 5.9. Core photograph taken in well BOR-31. The picture shows presence of vugs (blue arrows) and fractures (red arrows).

Figure 5.10 shows results for this case in the previously described theoretical model. The model confirms also in the case of well BOR-31 that perturbations of initial petrophysical properties are needed to improve simulation results and secure a good match between simulated and field-acquired resistivities. In the present case, we perform perturbations on permeability with minor perturbations of porosity from rock-core measurements. Porosity estimated from well-logs has a better agreement with that obtained from our simulation.

The above results confirm the application of simulation of mud-filtrate invasion to estimate permeability for vuggy and fractured carbonate reservoirs where the presence of fractures and interconnected vugs significantly improves reservoir quality. In the particular case of BOR-31, it was not possible to secure a better match in the separation observed between resistivity curves obtained from field data. One reason could be the high heterogeneity detected in core data and also the presence of clay minerals in pore throats. On the other hand, we have a limitation when we are applying simulation of mud-filtrate invasion considering a DLL tool. Nevertheless, general results of this case are reliable.

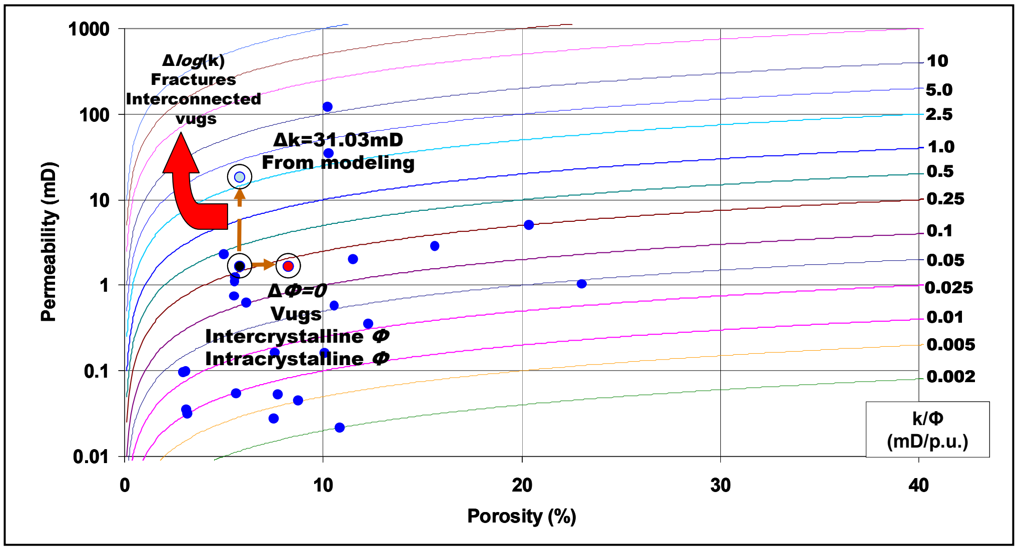

Figure 5.10. Application of the estimation method to the appraisal of secondary porosity and permeability in well BOR-31. Blue circles represent porosity and permeability obtained from rock-core data (plugs) in well BOR-31. Black circles indicate the initial average rock properties estimated from rock-core measurements. Red circles represent required perturbations of initial permeability and porosity due to the presence of fractures, interconnected vugs, intercrystalline and intracrystalline porosity or the combination of any of these features. The light blue circle identifies permeability and porosity obtained from mud-filtrate invasion modeling.

Finally, table 5.1 shows results obtained from the simulation of the mud-filtrate invasion compared to permeability obtained from other methods or measurements.

WELL	k_{Core} (MD)	$k_{Well-\log s}$ (MD)	k_{PTT} (MD)	k_{SMFI} (MD)
BOR-12	4.33	6.33	101.0	101.36
BOR-11	Not available	6.12	Not available	134.26
BOR-31	1.67	1.04	Not available	32.7

Table 5.1. Permeability results obtained from the simulation of mud-filtrate invasion and comparison to permeability values obtained from other methods or measurements.

In this table, k_{Core} represents permeability obtained from rock-core measurements, $k_{Well-\log s}$ is permeability estimated from well-log correlations, k_{PTT} stands for permeability calculated from pressure transient measurements, and k_{SMFI} is permeability estimated from simulation of the process of mud-filtrate invasion. All values are given in milidarcies (mD).

CHAPTER 6

Discussion of Results and Conclusions

The last chapter discusses results obtained from the study, including simulation results and their relation to the geological model. The discussion also includes a proposed theoretical model for the estimation of secondary porosity and permeability. In addition, we present an itemized list of sequential steps for the application of our proposed method of mud-filtrate invasion modeling to diagnose and quantify fractured and vuggy carbonate formations. Finally, we summarized the most important conclusions stemming from the thesis.

6.1 DISCUSSION OF RESULTS

According to Lucia's method (2007), porosity and permeability of carbonate reservoirs can be estimated by applying a relationship between porosity and permeability for particle-size groups in non-vuggy rocks. We implemented this approach to our data. In addition, we implemented a definition of rock types from both rock fabric and critical pore-throat radius using rock-core measurements to improve the petrophysical assessment. We believe that a combination of the previous two approaches permits a better petrophysical characterization of the matrix. However, it did not enable us to quantify the porosity and permeability of the vugs and fractures (important components that provide secondary porosity). Influence of these components was observed in the permeability of the petrophysical system inferred from pressure-transient tests, where the permeability was 24 times (BOR-12) and 146 (BOR-8) larger than the values measured on rock-core samples, which are mostly governed by one component of the system (matrix). This observation was confirmed with forward modeling of dual-laterolog logs. It is important to be aware of presence of vugs and fractures in “O BOR 2E” reservoir. They might lead to a significant difference between the petrophysical properties obtained from the two approaches as well as from the rock properties of the entire petrophysical system.

The previous remarks indicate that simulation of mud-filtrate invasion can be applied to estimate the secondary porosity and permeability due to vugs and fractures via the theoretical model described in Figure 6.1. Presence of non-connected vugs would be associated with those cases where significant changes of porosity are needed to fit the field data via forward modeling. Presence of connected vugs and fractures would be estimated for those cases where significant modifications of permeability from the base case would be needed to match the field measurements. There could also be a combination of both cases (Figure 6.1), as it was shown in the previous cases.

From the above observations, we developed and validated a method to estimate permeability of the entire petrophysical system (matrix, vugs, and fractures) considering the presence of components such as vugs and fractures. We implemented the method in key wells (rock-core data, pressure tests, conventional, and nonconventional well logs) for testing and calibration. These additional tests also improved the method and allowed us to identify vugs and/or fractures from field measurements by applying forward modeling of resistivity logs.

Results found in this research indicate that a key factor to appropriately simulate the mud-filtrate invasion process is to identify the presence of secondary permeability and porosity due to presence of fractures, interconnected vugs, intercrystalline and intracrystalline porosity, or a combination of any of these components. Therefore, the method assumes that laboratory measurements of rock-core samples are available from a key well. It is also necessary to count with image logs. In addition, fluid and mud properties must be available not only to secure a precise match between simulated and field resistivities but also to reduce the uncertainty of simulation results.

Permeability estimation is one of the most important tasks in reservoir characterization. Even though there are tested methods to estimate other important rock properties such as porosity and saturation, permeability, a tensorial property, remains the most difficult to estimate. In addition, the prediction of this property is exceedingly complicated in carbonate reservoirs. In clastic reservoirs, permeability is usually estimated through correlations between porosity and permeability measurements inferred from rock-core measurements and well logs in wells where both data are available. Then, one usually extrapolates the most appropriate correlation to estimate permeability values in wells that have no rock-core data. In carbonate reservoirs, it is difficult to infer such direct relationships. Presence of other components such as vugs and fractures that modify the permeability of the system can be an important factor to reliable estimate permeability values. In carbonate reservoirs that exhibit a triple-porosity system, permeability values from rock-core measurements only represent the permeability of the matrix and not the permeability of the entire petrophysical system.

Therefore, results found in our research favor the application of simulation of mud-filtrate invasion process to reliable estimate the permeability of the entire system. Despite difficulties and limitations associated with uncertainty of some parameters, and high variations of resistivity due to presence of heterogeneities in some cases, the method described in this thesis allows the reliable estimation of permeability for fractured and vuggy carbonate reservoirs. Rock-core measurements, pressure-transient tests, and advanced well logs such as image logs would be necessary to calibrate the initial estimation of petrophysical properties in key wells. They would also minimize the uncertainty associated to estimation of permeability and porosity values. As a result, the lack of such information would be a limitation in securing an accurate estimation of permeability and porosity values.

Finally, we present an itemized list of sequential steps for our proposed method of mud-filtrate invasion modeling to diagnose and quantify fractured and vuggy carbonate formations:

1. Define rock types from both rock fabric and critical pore-throat radius using rock-core measurements.
2. Identify the presence of secondary permeability and porosity due to the presence of fractures, interconnected vugs, intercrystalline and intracrystalline porosity, or the combination of any of these components.
3. Define flow units and layers for the simulation from the initial petrophysical assessment.
4. Estimate initial rock-properties (porosity, permeability and water saturation) from well-log correlations and through integrated petrophysical assessment.

5. Define mud properties from mud logs, drilling reports, and mud-filtrate invasion tests.
6. Calculate and/or measure capillary pressure and relative permeability from rock-core measurements and model these properties with Brooks-Corey's equations and parameters.
7. Input petrophysical, fluid, and mud properties into UTFET simulation software.
8. Perform numerical simulation of mud-filtrate invasion process to obtain initial permeability and porosity values for each layer.
9. Progressively make perturbations to the permeability of each layer until securing a match between simulated and measured apparent resistivity curves.
10. In some cases, a perturbation of initial porosity will be necessary to match the measured apparent resistivity due to the presence of vugs or non-connected pore space.
11. Compare the results obtained with permeability estimated from pressure transient measurements and observations of fractures and vugs from core analysis and image logs.
12. The average permeability and porosity has been estimated for each layer when there is a match between simulated and measured apparent resistivity curves.

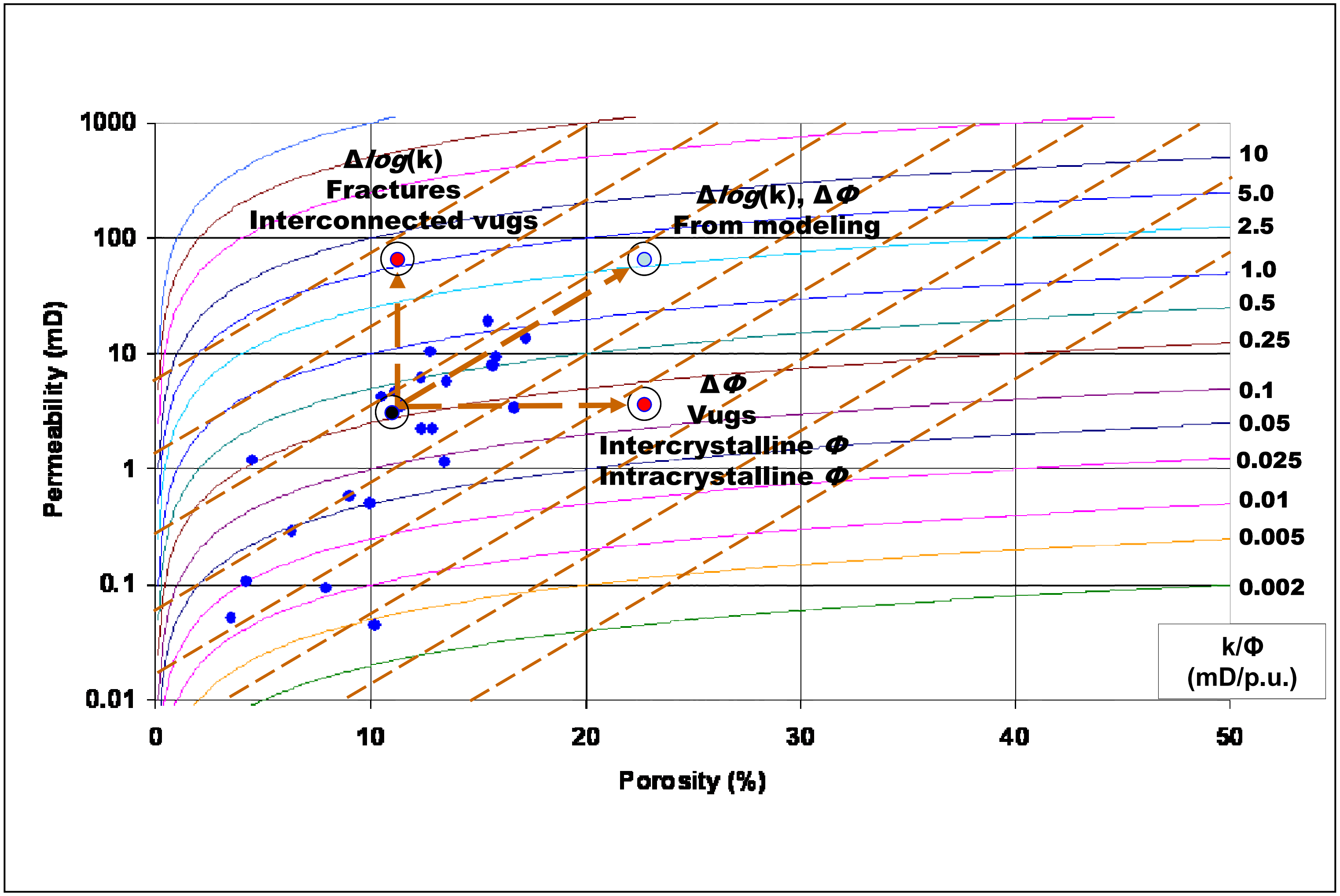
Δ*log*(k)
Fractures
Interconnected vugs
Δ*log*(k), ΔΦ
From modeling
ΔΦ
Vugs
Intercrystalline Φ
Intracrystalline Φ
Permeability (mD)
1000
100
10
1
0.1
0.01
Porosity (%)
0
10
20
30
40
50
10
5.0
2.5
1.0
0.5
0.25
0.1
0.05
0.025
0.01
0.005
0.002
k/Φ
(mD/p.u.)

Figure 6.1. Proposed method to diagnose and quantify secondary porosity and permeability. Blue circles represent porosity and permeability obtained from rock-core data or estimated from well-log correlations. Black circles identify the initial average rock properties obtained from rock-core measurements or well-log correlations. Red circles identify perturbations of initial permeability and porosity due to presence of fractures, interconnected vugs, intercrystalline and intracrystalline porosity, or a combination of any of these components. The light blue circle identifies permeability and porosity obtained from the simulation of mud-filtrate invasion. Orange dashed lines identify changes of initial permeability obtained from the simulation of mud-filtrate invasion process by matching the available apparent resistivity logs.

6.2 CONCLUSIONS

Resistivity logs are highly influenced by the porosity of the entire petrophysical system. Therefore, the use of such measurements enabled us to quantify secondary porosity due to vugs and fractures via forward modeling of resistivity logs integrated with rock-core measurements and non-conventional logs. The previous remarks indicate that simulation of mud-filtrate invasion can be applied to estimate secondary porosity and permeability due to vugs and fractures.

In clastic reservoirs, permeability is commonly estimated from relationships between porosity and permeability measurements performed on rock-core samples and well logs acquired in wells where both data are available. Subsequently, one extrapolates the most appropriate relationship to estimate values of permeability in wells devoid of rock-core measurements. In carbonate reservoirs, especially in fractured and vuggy reservoirs, a deterministic correlation is often difficult to ascertain. In many cases, presence of other components (vugs and fractures) modifies the permeability of the system. As it has been previously emphasized, the carbonate reservoir considered in this thesis is regarded a triple-porosity system (matrix + vugs + fractures). Therefore, permeability values from rock-core measurements will only honor the permeability of the matrix and not the permeability of the entire petrophysical system.

We have developed and successfully tested a new method to diagnose and quantify fractured and vuggy carbonate formations via the simulation of the process of mud-filtrate invasion. The method was applied in a set of three wells drilled in a carbonate reservoir in the Escandalosa formation of southwest Venezuela. Two of our three cases included rock-core measurements that enabled the validation of the method. In addition, pressure transient measurements and image logs combined with core data enabled us to identify the presence of vugs and fractures that significantly contributed to the total porosity and permeability of the petrophysical system. Matching of apparent resistivity logs was performed after successive perturbations of porosity and/or permeability. These perturbations were used to diagnose presence of secondary porosity and permeability. Permeability estimated from our three cases was consistent with permeability values estimated from pressure transient measurements that are believed to be the best representation of the permeability of the entire petrophysical system.

Based on observations of core data and image logs, vugs are the major components of the secondary porosity while fractures and interconnected vugs are responsible for most of the permeability, especially in zones with a tight matrix. On the other hand, permeability obtained from rock-core measurements is in general representative of only one component of the system (matrix).

Appendix 1

Detailed Inventory of Well-Logs Available For This Reservoir

Table A.1 is a detailed inventory of well-logs available for this study. It also identifies those wells with rock-core measurements. The terminology used to designate each well log in this table is explained in the nomenclature section.

Well	SP	Caliper	GR	GR sp	Rs	Rm	Rt	Lat.	RHOB	NPHI	PEF	DT	Core	NMR	Others	Type of Mud	Pressure Transient	Resistivity Tool
BOR-1X	X	X	X	X	X		X	X	X	X		X			Dipmeter, RFT, Wall Samples	Polymer		Laterolog-HLS
BOR-2E	X	X	X	X	X	X	X	X	X	X	X	X			Mineralogic	Cationic	x	Laterolog
BOR-3E	X	X	X	X		X	X		X	X		X	X			Lignosulfate		Induction-DIPL-BA
BOR-4E	X	X	X			X		X	X	X		X			Image	OBM		Induction-DIPL-BA
BOR-5E			X	X	X	X	X		X	X		X	X	X		OBM		Induction-HRI-HLS
BOR-6E		X	X	X		X	X		X	X		X			Image	OBM		Induction-HRI-HLS
BOR-7			X							X					C/O	Water Gel		C/O SLB
BOR-8		X	X			X	X		X	X		X	X			OBM	x	Induction-HRI-HLS
BOR-9		X	X		X	X	X		X	X	X			X	Image, MDT, 6-Arms Caliper	OBM		AIT-B-SLB
BOR-10	X	X	X	X	X	X	X		X	X	X	X			Check Shot	Flow Pro		Laterolog-SLB
BOR-11	X	X	X	X	X	X		X	X	X		X			Image	Flow Pro		Laterolog-SLB
BOR-12X		X	X	X			X	X	X	X	X		X			Politex HT Drill	x	Laterolog-SLB
BOR-13			X	X				X	X	X		X		X	Image	Politex		Laterolog-BA
BOR-14		X	X		X		X	X	X	X	X		X		NMR Core Analysis	Politex		Laterolog-SLB-DLT-E
BOR-15		X	X		X	X	X			X	X					OBM		AIT-SLB
BOR-16		X	X		X	X	X		X	X	X					OBM		AIT-SLB
BOR-17		X	X		X	X	X		X	X	X	X			6 Arm Caliper, SFT, CHECK SHOT	OBM		Induction-HRI-HLS
BOR-18		X	X		X	X	X		X	X	X			X	Form Tester (RDT)	OBM		Induction-HRI-HLS
BOR-19		X	X		X	X	X		X	X	X			MRIL	Image	OBM		Induction-HRI-HLS
BOR-20		X	X		X	X	X		X	X	X				Image	OBM - Air WBM		Induction-HRI-HLS
BOR-21			X												ARP/APS(LWD) Image	OBM		LWD-SLB
BOR-22		X	X		X	X	X		X	X	X			X	Image	OBM		AIT-M-SLB
BOR-23		X	X		X	X	X		X	X	X			X	Image, Mineralogical	OBM		AIT-C-SLB
BOR-24		X	X		X	X	X		X	X	X			X	Image, Mineralogical	OBM		AIT-M-SLB
BOR-25		X	X		X	X	X		X	X	X	X				OBM		Induction-STI-PD
BOR-26		X	X			X	X		X	X	X				Image	OBM - Air WBM		Induction-STI-PD
BOR-27		X	X			X	X		X	X	X				Image	OBM - Air WBM		Induction-STI-PD
BOR-31		X	X		X	X	X	X	X	X	X	X	X	X	Image, Mineralogical, 6-Arms Caliper, MDT, Sonic Scanner	OBM - Air WBM		HRLA-SLB
BOR-33		X	X		X	X	X	X	X	X	X	X		X	Image, Mineralogical, 6-Arms Caliper, MDT, Sonic Scanner	OBM - Air WBM		HRLA-SLB

* Data of wells BOR-28 to BOR-30, BOR-32, and other wells drilled after BOR-33 were not available for this study.

Table A.1. Detailed inventory of well-logs available for this study

Appendix 2

Brooks-Corey Equations and Summary of Parameters Considered For the Modeling of Capillary Pressure and Relative Permeability

This appendix describes the parameters included in the Brooks-Corey equations. It also summarizes the parameters used for modeling capillary pressure and relative permeability.

For the numerical simulation, we apply Brooks-Corey's model (Corey, 1994) adjusted to rock-core measurements as shown in Figure 4.1 for capillary pressure and relative permeability. Brooks and Corey (1966) introduced a method to estimate capillary pressure of a two-phase fluid mixture. The saturation-dependent capillary pressure can be calculated with the equation:

$$P_c = P_c^o \sqrt{\frac{\phi}{k}\left(1 - S_N\right)^{e_p}}\ , \qquad \text{(B.1)}$$

where P_c is the capillary pressure, P_c^o is the coefficient for capillary pressure, ϕ is porosity, k is permeability, e_p is the pore-size distribution exponent, and S_N is the normalized wetting phase saturation, given by:

$$S_N = \frac{S_w - S_{wr}}{1 - S_{wr} - S_{nwr}}\ , \qquad \text{(B.2)}$$

where S_{wr} and S_{nwr} are the residual wetting and non-wetting phase saturations, respectively, and S_w is the wetting-phase saturation.

Relative permeability curves for multi-phase imbibition and drainage in the saturated zone can be estimated through the equations:

$$k_{rw} = k_{rw}^{0} S_{N}^{e_w} , \tag{B.3}$$

and

$$k_{rnw} = k_{rnw}^{0} \left(1 - S_N\right)^{e_{nw}} , \tag{B.4}$$

where k_{rw} and k_{rnw} are wetting and non-wetting phase relative permeabilities respectively, k_{rw}^{0} and k_{rnw}^{0} are relative permeability end points, and e_w and e_{nw} are empirical exponents for each fluid phase. Figure 4.1 shows the match of Brooks-Corey's oil-brine capillary pressure and relative permeability to laboratory core measurements acquired in one of the wells used in the thesis.

Finally, we give a summary of the parameters used in the simulations considered in this thesis. Table B.1 shows formation properties used for the simulation of the process of mud-filtrate invasion. Table B.2 gives the critical properties of binary-components used for the simulation of mud-filtrate invasion.

Variable	Units	Value
Initial formation pressure	psi	4,500
Mud-filtrate viscosity	cp	1.50
Oil density	lb/ft^3	55.38
Maximum invasion time	days	2.00
Maximum invasion flow rate	ft^3/d/ft	0.079
Temperature	°F	275
Formation outer boundary	ft	2000
Residual water saturation	fraction	0.52
Residual oil saturation	fraction	0.21

Table B.1. Formation properties used for the simulation of mud-filtrate invasion.

Property	Units	FHC$_1$	MC$_{16}$
Critical Temperature	°F	708.0	822.4
Critical Pressure	psi	249	245
Acentric Factor	-	0.530	0.7112
Molar Weight	lb/mol	238	222
Viscosity	cp	2.18	1.5

Table B.2. Critical properties of binary-components used for the simulation of mud-filtrate invasion.

Nomenclature

a : Tortuosity factor, dimensionless

C_{sh} : Content of shale

DT : Sonic log, (µs/ft)

e_{nw} : Empirical exponent for k_{rnw}, dimensionless

e_{w} : Empirical exponent for k_{rw}, dimensionless

GR : Gamma ray, (API units)

GR sp : Spectral gamma ray, (API units)

k : Permeability, (mD)

k_{air} : Uncorrected air permeability, (mD)

k_{rnw} : Non-wetting phase relative permeability, dimensionless

k_{rw} : Wetting phase relative permeability, dimensionless

k_{rnw}^{0} : Relative permeability end point for k_{rnw}, dimensionless

k_{rw}^{0} : Relative permeability end point for k_{rw}, dimensionless

k_{Core} : Permeability obtained from rock-core measurements, (mD)

k_{PTT} : Permeability calculated from pressure transient measurements, (mD)

k_{SMFI} : Permeability estimated from simulation of mud-filtrate invasion simulation, (mD)

$k_{Well-\log s}$: Permeability estimated from well-logs correlations, (mD)

m : Cementation exponent, dimensionless

n : Saturation exponent, dimensionless

NPHI : Neutron log, (fraction)

NMR : Nuclear magnetic resonance log

PEF : Photoelectric factor log, (barn/elect)

P_c : Capillary pressure, (psi)

P_c^o : Coefficient for capillary pressure, dimensionless

r : Pore-throat radius (µm)

r_{35} : Pore aperture radius corresponding to the 35th percentile, (µm)

RHOB : Density log, (g/cm³)

R_t : True formation resistivity, (Ohm-m)

R_w : Connate water resistivity, (Ohm-m)

R_{xo} : Flushed-zone resistivity, (Ohm-m)

S_N : Normalized wetting-phase saturation, dimensionless

SP : Spontaneous potential log, (mv)

S_w : Water saturation, (fraction)

V_{DS} : Volume of dolomite, (fraction)

V_{SS} : Volume of sandstone, (fraction)

V_{LS} : Volume of limestone, (fraction)

V_{sh} : Volumetric concentration of shale, (fraction)

Greek symbols

ϕ : Porosity, (fraction)

θ : Contact angle between the fluid interface and the rock, (degrees)

ρ_1, ρ_2 : Fluid density, (g/cm³)

ρ_{ma} : Matrix density, (g/cm³)

σ : Interfacial tension, (dynes/cm)

ρ_{bDS} : Reading of density log of dolomite

ρ_{bLS} : Reading of density log of limestone

ρ_{bSS} : Reading of density log of sandstone

ρ_{bSh} : Reading of density log of shale

ρ_{bF} : Reading of density log of the fluid

ϕ_{D} : Porosity obtained from bulk density log without corrections by content of shale

ϕ_{DC} : Porosity obtained from bulk density log corrected by content of shale

ϕ_{Dsh} : Bulk density log response in a shale formation

ϕ_{e} : Effective porosity

ϕ_{NC} : Porosity obtained from neutron log corrected by content of shale

ϕ_{N} : Porosity obtained from neutron log without corrections by content of shale

ϕ_{Nsh} : Neutron log response in a shale formation

References

Aguilera, R., “Naturally Fractured Reservoirs,” Second Edition, Penwell Books, 1995.

Archie, G., “The Electrical Resistivity Logs as an Aid in Determining Some Reservoir Characteristics”. Trans AIME, 1942

Babadagli, T., and Al-Salmi, S., “A Review of Permeability-Prediction Methods for Carbonate Reservoirs Using Well-Log Data,” SPE Reservoir Evaluation & Engineering, April 2004.

Bona, N., Radaelli, F., Ortenzi, A., De Poli, A., Peduzzi, C., and Georgiani, M., “Integrated Core Analysis for Fractured Reservoirs: Quantification of the Storage and Flow Capacity of Matrix, Vugs, and Fractures,” SPE Reservoir Evaluation & Engineering, August 2003.

Coates, G. and Dumanoir, J., “A New Approach to Improved Log-Derived Permeability,” The Log Analyst, January 1974.

Corey, A., “Mechanics of Immiscible Fluids in Porous Media,” Water Resource Publications, 1994.

CORPRO Systems Ltd., “Geological Study of Tectonic and Sedimentary Structures Well: BOR-12,” November 2000.

CORPRO Systems Ltd., “Geological Study of Tectonic and Sedimentary Structures Well: BOR-14,” May 2001.

Dewan, J.T., “Essentials of Modern Open-Hole Log Interpretation,” PennWell Publishing Company, 1983.

Dussan, E.B., Anderson, B.I., and Auzerais, F.M., “Estimating Vertical Permeability From Resistivity Logs,” in Proceedings of the SPWLA 35th Annual Logging Symposium, Tulsa, Ok, June 1994.

ELAN User Guide, Schlumberger Information Solutions (SIS), 2003.

Gomaa, N., Al-Alyak, A., Ouzzane, D., Saif, O., Okuyiga, M., Allen, D., Rose, D., Ramamoorthy, R., and Bize, E., “Case Study of Permeability, Vug Quantification, and Rock Typing in a Complex Carbonate,” in Proceedings of the 2006 SPE Annual Technical Conference and Exhibition, San Antonio, TX, September 2006.

Hurley, N.F., Zimmermann, R.A., and Pantoja, D., "Quantification of Vuggy Porosity in a Dolomite Reservoir from Borehole Images and Core, Dagger Draw Field, New Mexico," in Proceedings of the 1998 SPE Annual Technical Conference and Exhibition, San Antonio, TX, September 1998.

HRLA High-Resolution Laterolog Array Tool Specifications, Schlumberger, April 2000.

Interactive Petrophysics (IP) User Guide, Schlumberger Information Solutions (SIS), 2004.

Jennings, J., and Lucia, F.J., "Predicting Permeability From Well Logs in Carbonates With a Link to Geology for Interwell Permeability Mapping," SPE Reservoir Evaluation & Engineering, August 2003.

Kupecz, J., Sorondo, J., Rojas, L., Petito, M., Chang, R., Calderon, P., Solórzano, E., and Hernandez, E., "Quantitative Characterization of a Mixed Carbonate-Siliciclastic Interval for Reservoir Simulation: Escandalosa Formation, "O" Member, Barinas-Apure Basin, Venezuela," AAPG Bulletin, Vol. 84, No. 13 (Supplement), 2000.

Lucia, F.J., "Carbonate Reservoir Characterization - An Integrated Approach," Second Edition, Springer, 2007.

Lucia, F.J., "Characterization of Petrophysical Flow Units in Carbonate Reservoirs: Discussion," AAPG Bulletin, Vol. 83, No. 7, July 1999.

Lucia, F.J., "Petrophysical Parameters Estimated From Visual Descriptions of Carbonate Rock: A Field Classification of Carbonate Pore Spaces," JPT, March 1983.

Lucia, F.J., "Rock-Fabric/Petrophysical Classification for Carbonate Pore Space for Reservoir Characterization," AAPG Bulletin, Vol. 79, No. 9, September 1995.

Malik, M., Salazar, J., Torres-Verdín, C., Wang, G.L., Lee, H.J., and Sepehrnoori, K., "Influence of Petrophysical and Fluid Properties on Array-Induction Measurements Acquired in the Presence of Oil-Base Mud-Filtrate Invasion," in Proceedings of the SPWLA 48th Annual Logging Symposium, Austin, TX, June 2007.

Martin, A.J.; Solomon, S.T.; Hartmann, D.J.; "Characterization of Petrophysical Flow Units in Carbonate Reservoirs: Reply," AAPG Bulletin, Vol. 83, No. 7, July 1999.

Méndez, J., "Caracterización Sedimentológica del Miembro "O" en el Área de Borburata, Formación Escandalosa," PDVSA Internal Report, May 2002.

Moore, C., "Carbonate Reservoirs: Porosity Evolution and Diagenesis in a Sequence Stratigraphic Framework," Elsevier, 2001.

Omni Laboratories, Inc; "Sedimentological and Reservoir Characterization Study of PDVSA BOR-31 Well, Borburata Field, Venezuela," Client Report, 2007.

PDVSA "Análisis de Núcleos de los Pozos BOR-12 y BOR-14 en el Yacimiento O BOR 2," Internal Report, 2002.

PDVSA "Factibilidad de Aplicar Recuperación Secundaria en el Yacimiento O BOR 2, Primera Fase," Internal Report, 2003.

PDVSA "Modelo Estructural y Análisis de Sísmica 3D del Yacimiento O BOR 2, Campo Borburata," Intevep Internal Report, 2004.

Pittman, E.D.; "Relationship of Porosity and Permeability to Various Parameters Derived from Mercury Injection-Capillary Pressure Curves for Sandstone," AAPG Bulletin, Vol. 76, No. 2, February 1992.

Ramirez, T.R., Torres-Verdín, C., Lee, H.J., and Wang, G.L., "Interactive Assessment of the Sensitivity of Well Logs to Static and Dynamic Petrophysical Properties of Rock Formations," in Proceedings of the 2006 AAPG International Conference and Exhibition, Perth, Australia, November 2006.

Rangel, J., "Modelo Petrofísico para la Identificación de Petrofacies en Rocas Carbonáticas, Compararlas con sus Facies Sedimentarias y Extrapolar el Modelo haciendo Uso de Redes Neuronales" (Formación Escandalosa Miembro "O" Campo Borburata Cuenca Barinas – Apure)," Universidad de los Andes, 2003.

Salazar, J.M., Malik, M., Torres-Verdín, C., Wang, G.L., and Duan, H., "Fluid Density and Viscosity Effects on Borehole Resistivity Measurements Acquired in the Presence of Oil-Based Mud and Emulsified Surfactants," in Proceedings of the 2007 SPE Annual Technical Conference and Exhibition, Anaheim, California, November 2007.

Salazar, J., Torres-Verdín, C., Alpak, F., and Klein, J., "Estimation of Permeability from Borehole Array Induction Measurements: Application to the Petrophysical Appraisal of Tight Gas Sands," Petrophysics Vol. 47, December 2006.

Salazar, J.M., Torres-Verdín, C., and Sigal, R., "Assessment of Permeability from Well Logs Bases On Core Calibration and Simulation of Mud-Filtrate Invasion," Petrophysics Vol. 46, No. 6, December 2005.

Salazar, J.M., Torres-Verdín, C., Wang, G.L., and Lee, H.J., "Combined Simulation and Inversion of SP and Resistivity Logs for the Estimation of Connate Water Resistivity and Archie's Cementation Exponent," submitted for publication in Geophysics, September 2007.

Tiab, D., and Donaldson, E., “Petrophysics Theory and Practice of Measuring Reservoir Rock and Fluid Transport Properties,” Second Edition, Gulf Publishing Company, 2004.

Timur, A., “An Investigation of Permeability, Porosity, and Residual Water Saturation Relationship for Sandstone Reservoirs,” The Log Analyst, Vol. 9, No. 4, July 1968.

Tixier, M., “Evaluation of Permeability from Electric-Log Resistivity Gradients”, Oil and Gas Journal, June 1949.

Wang, G.L. and Torres-Verdín, C., “Fast Numerical Simulation and Inversion of SP and Borehole Induction Measurements to Estimate Resistivity and Permeability,” in Proceedings of the SPWLA 48th Annual Logging Symposium, Austin, TX, June 2007.

Wu, J., Torres-Verdín, C., Sepehrnoori, K., and Proett, M.A., “The Influence of Water-Base Mud Properties and Petrophysical Parameters on Mudcake Growth, Filtrate Invasion, and Formation Pressure,” Petrophysics Vol. 46, No. 1, February 2005.

Wyllie, M. and Rose, W., “Some Theoretical Considerations Related to the Quantitative Evaluation of the Physical Characteristics of Reservoir Rock from Electric Log Data,” Trans., AIME, Vol. 189, 1950.

Vita

Luis Javier Miranda was born in Maracaibo, Venezuela on December 12, 1976, the first son of Graciela de Jesus Lamby de Miranda and Luis Ramon Miranda Olmedo. After graduating as a petroleum engineer with academic distinction at La Universidad del Zulia, Maracaibo, Venezuela, in 1998, he immediately started working for PDVSA (Venezuelan National Oil Company) in Barinas, Venezuela. During 2000 he attended the Formation Evaluation School in PDVSA Eastern Division, in Puerto La Cruz, Venezuela. During the following years he was working as a Petrophysicist at PDVSA South Division, in Barinas, Venezuela. In 2006, he entered The Graduate School at The University of Texas at Austin to pursue a Master of Science in Petroleum Engineering.

Permanent address: Urb. Los Lirios, Calle Las Rosas, F-15, Barinas, Venezuela 5201

This thesis was typed by the author.